1 **Multimodal and multisensory coding in the *Drosophila* larval peripheral**

2 **gustatory center**

3

4

5 G. Larisa Maier[1], Marjan Biočanin[2], Johannes Bues[2], Felix Meyenhofer[1], Clarisse Brunet

6 Avalos[1], Jae Young Kwon[3, 4], Bart Deplancke[2, 4] and Simon G. Sprecher[1,4,5]

7

8 [1]Department of Biology, University of Fribourg, 1700 Fribourg, Switzerland

9 [2]Laboratory of Systems Biology and Genetics, Institute of Bioengineering, School of Life

10 Sciences, EPFL and Swiss Institute of Bioinformatics (SIB), 1015 Lausanne, Switzerland

11 [3] Department of Biological Sciences, Sungkyunkwan University, Suwon 16419, Republic of

12 Korea

13

14 [4] J.Y.K., B.D. and S.G.S. are co-senior authors.

15 [5] To whom correspondence should be addressed. Email: simon.sprecher@unifr.ch

Abstract

The ability to evaluate food palatability is innate in all animals, ensuring their survival. The external taste organ in *Drosophila* larvae is composed of only few sensory neurons but enables discrimination between a wide range of chemicals and displays high complexity in receptor gene expression and physiological response profile. It remains largely unknown how the discrepancy between a small neuronal number and the perception of a large sensory space is genetically and physiologically resolved. We tackled dissection of taste sensory coding at organ level with cellular resolution in the fruit fly larva by combining whole-organ calcium imaging and single-cell transcriptomics to map physiological properties and molecular features of individual neurons. About one third of gustatory sense neurons responded to multiple tastants, showing a rather large degree of multimodality within the taste organ. Further supporting the notion of signal integration at the periphery, we observed neuronal deactivation events within simultaneous neighboring responses, suggesting inter-cellular communication through electrical coupling and thus providing an additional level in how neurons may encode taste sensing. Interestingly, we identified neurons responding to both mechanical and taste stimulation, indicating potential multisensory integration. On a molecular level, chemosensory cells show heterogeneity in neuromodulator expression. In addition to a broad cholinergic profile, markers on dopaminergic, glutamatergic or neuropeptidergic pathways are present either in distinct cell populations or are seemingly co-expressed. Our data further extend the sensory capacity of the larval taste system pointing towards an unanticipated degree of multimodal and multisensory coding principles.

Introduction

Taste sensing provides the innate ability in all animals to avoid toxic or deleterious food ingestion and to choose a nutritious diet. The fruit fly larva is able to discriminate between a large range of different gustatory cues (1), being – similarly to humans – repelled by bitter tastants (2-4) as possible signals of toxic food, and attracted by sweet and certain amino acids (5-7), indicators of a nutritious diet. Distinct from mammals where hundreds of taste cells are assembled in taste buds on the tongue, the larva disposes of very few gustatory sense neurons (GSNs) at the periphery (8, 9), raising the question of how does a small neuronal population encode a large palette of cues.

 Distinct models of sensory coding have emerged for taste perception. According to the labeled-line model, each cell within a mammalian taste bud is tuned to one of the 5 basic tastes – sweet, umami, bitter, sour and salt (10-13). This model relies to a large extent on the existence of a best stimulus concentration (14) but varying the concentration of a given tastant alters the number of responding cells and afferent sensory neurons, often increasing the proportion of multituned neurons (15). Moreover, taste cells within a bud have been shown to communicate with each other through purinergic signaling (16), entailing coexistence of narrowly and broadly tuned taste sensing cells (17) and signal integration at the periphery, distinct from a strictly segregated taste sensing model.

In *Drosophila* taste sensing has been described in accordance with a labeled-line model, as sweet, bitter and water perception localize in separate populations of peripheral GSNs (18-22). However, additional tastes such as salt, fatty acid, carbonation, polyamines or amino acids partially overlap onto sweet or bitter sensing GSNs by means of specific added-on

62   receptor expression (23-30), suggesting a model of taste sensing with both narrowly and more

63   broadly tuned cells, similar to mammals.

64   The peripheral gustatory system in the *Drosophila* larva presents many similarities with the

65   adult fly, such as the sensillar organization of dendrites, presence of both internal and external

66   chemosensory organs (31), as well as cue detection through the same chemoreceptor gene

67   families – GRs (Gustatory Receptors), IR (Ionotropic Receptors), PPKs (pickpocket) or TRPs

68   (Transient Receptor Potential) (29, 32-38). On the other hand, larval taste processing presents

69   developmental stage particularities, considering that the number of GSNs is much lower than

70   in adult flies and many receptors are larva-specific (39, 40).

71   The main chemosensory organs in *Drosophila* larva are located at the tip of the head,

72   represented by ganglia of bipolar sensory neurons (Fig.1A) (41). External organs include the

73   terminal organ ganglion (TOG) – with main taste, but also mechano- and thermo-sensory

74   function, the dorsal organ ganglion (DOG) – with primary olfactory role, and the smaller,

75   generally uncharacterized ventral organ ganglion (VOG) – with associated taste function (8).

76   Sensory neurons in these ganglia extend dendrites to the periphery in direct contact with the

77   environment and axonal projections into defined regions of the brain. Conversely, internal

78   chemosensory organs called ventral, dorsal and respectively posterior pharyngeal sensories

79   (VPS, DPS, PPS) are located on the pharyngeal tube where they project their dendrites (42),

80   therefore functionally associated with taste sensing during food ingestion.

81   Thanks to the 1 to 1 receptor to neuron expression in the DOG, functional dissection of the 21

82   olfactory sensory neurons was achieved using corresponding Gal4 lines (43-47). In contrast,

83   the neighboring TOG, main external larval taste center, comprises more than 30 GSNs out of

84   which only 7 neuronal identities (C1-C7) have been mapped and can be traced using

85   individual Gal4 lines (Fig.1B) (39, 48, 49). Characterization of single larval GSNs has

86 revealed multimodality and even taste integration of opposed valence within one GSN (48),

87 but the general taste sensing logic in this animal remains largely unexplored.

88 We here delve into sensory tuning diversity of TOG neurons by using whole-organ in-vivo

89 calcium imaging recordings on larvae expressing genetically encoded calcium sensors. To

90 gain insight into molecular components of TOG and DOG neurons we employed DisCo, a

91 novel approach that enables single-cell RNA sequencing of low input samples (50). Our

92 findings provide insights into fundamental aspects of taste sensory coding. First, we show that

93 roughly one third of responding GSNs are activated by more than one taste modality, while

94 conversely, single tastants generally elicit responses in several neurons. Interestingly, we

95 detected neuronal deactivation responses, distinct from canonical calcium imaging signals,

96 which occurred within concomitant firing in adjacent neurons, as described for electrical

97 coupling in the adult fly olfactory system (51, 52). Using DisCo and immunostainings, we

98 identified distinct and common molecular markers in TOG/DOG neurons. While it was

99 known that larval chemosensory neurons are cholinergic (53), we found that they are also

100 glutamatergic and dopaminergic, and, similar to the central nervous system (CNS) (54),

101 neurons may also co-express neurotransmitter markers. Lastly, we detected expression of

102 mechanosensory receptor genes and, intriguingly, GCAMP recordings showed activation to

103 both mechanical and chemical stimulation in some neurons, implying multisensory

104 integration at single cell level. Taken together, our observations of the larval external

105 gustatory organ bring evidence of multimodality, possibly inter-cellular communication

106 through electric coupling, heterogeneous expression of neurotransmitter markers and

107 mechanosensory features in GSNs.

Results

Whole organ larval taste recordings with single cell resolution

Due to the sparse availability of Gal4 lines for individual GSN labeling in the larva, assessing an overview of peripheral taste coding by tackling single neurons entails limitations. We therefore undertook characterization of TOG neurons by means of a whole-organ approach.

First, we performed immunostainings on individual GSNs expressing *myr*:*GFP* (Fig.1C & D). Structural flexibility of this tissue entails variability across samples but we noted the 7 previously identified GSNs maintained a relatively stereotypical localization between stainings (n≥3) (Fig1C). This allowed assembling 3D locations of the 7 GSNs, serving as approximation map of their respective position within the organ (Fig.1D).

Further, we performed whole-organ calcium imaging recordings by expressing cytoplasmic GCaMP6m (55) and nuclear RFP (56) reporters in all neurons driven by *nSyb*-Gal4 (Fig.1E). The use of a nuclear reporter as cellular landmark was critical for whole organ recordings, as solely a cytoplasmic fluorophore would not sufficient for efficient segmentation due to low baseline fluorescence intensity in some cells and to ambiguous delimitation between neighboring somata. As previously described (57), we made use of a customized microfluidic chamber for chemical stimulation while recording physiological responses of all GSNs in a semi-intact larval preparation, and we subsequently developed a data processing pipeline for whole organ recordings (Suppl.Fig.1).

One third of responding GSNs show taste multimodality

131   We first tested two distinct series of chemicals each containing 5 substances belonging to the

132   5 canonical taste categories: sweet, bitter, sour, amino acids and salt. Substances and

133   concentrations were chosen according to former studies (48, 58) (Table1, Fig.2A, see

134   Methods). Out of all responding neurons across 15 total recorded organs, 66% showed

135   activation to only one tastant per animal and most unimodal responses were recorded to

136   sucrose and high salt (Fig.2A, uni-taste/cell). In line with our previous findings that some

137   GSNs are multimodal (48), the remaining 34% of responding neurons were activated by more

138   than one substance (Fig.2A, Suppl.File1), showing that several larval GSNs have the capacity

139   to respond to different taste categories. The top 5 taste response combinations mapping to one

140   neuron (Fig.2A, multi-taste/cell) were: sucrose and valine/arginine (sweet + amino acid,

141   17%), sucrose and citric acid (sweet + sour, 17%), citric acid and high salt (sour + high salt,

142   14%), sucrose and high salt (sweet + high salt, 14%) and finally sucrose and

143   denatonium/quinine (sweet + bitter, 14%). Interestingly, sucrose was the tastant

144   corresponding to most uni-taste/cell responses but also to most frequent taste combinations of

145   multi-taste/cell.

146   Next, we expanded the number of gustatory cues used for GSN stimulation by using groups of

147   tastants for sweet, bitter, amino acid and salt taste categories (Fig.2B, Suppl.Table 1). To

148   begin with, we tested 2 groups of sugars, chosen as monosaccharides (fructose, glucose,

149   arabinose, mannose, galactose), and respectively disaccharides (sucrose, trehalose, maltose,

150   lactose, cellobiose). We calculated a rounded 74% of sugar-responsive neurons to be activated

151   by either monosaccharides (41%) or disaccharides (33%), and a rounded 25% by both groups

152   (Fig.2B, upper left panel).

153   For salt taste stimulation we mixed NaCl and KCl for a final concentration of 50mM for low

154   salt group and respectively 1M for high salt group. We observed a low percentage of cell

7

155   activation overlap among salt-responding cells, 20% being activated by both groups while the

156   rest responded either to high salt (56%) or to low salt (24%).

157   The 20 proteinogenic amino acids were compiled in 4 groups (A, B, C and D) as previously

158   described by Park et al. (59) (Suppl.Table 1). 38% amino acid-responding neurons showed

159   activation to 2 or more amino acid groups. Similar percentages were observed for animals

160   stimulated with all 8 groups (2 sugar, 2 salt and 4 amino acid units), with up to 40% neurons

161   responding to at least 2 different taste modality groups (Fig.2B upper right panel).

162   Bitter tastants were randomized in 2 groups of 4 substances each (Suppl.Table 1): DSoTC

163   group (denatonium benzoate, sucrose octaacetate, theophylline, coumarin), and respectively

164   QLSC group (quinine, lobeline, strychnine, caffeine). Among cells responsive to bitter

165   stimulation we observed a bigger fraction of cells activated by DSoTC group (55%) than by

166   QLSC (30%). In animals tested for sweet and bitter taste response, the percentage of cells

167   activated by both sugar and bitter groups was of 30% (Fig.2B, lower panels), in agreement

168   with cell integration of tastants with opposite valence.

169

Taste stimulation can elicit either activation or deactivation signals in GSNs

171   While canonical responses of GSNs to taste cues entail a rise of GCaMP fluorescence, we

172   also detected neuronal responses characterized by a fluorescence intensity decrease. For

173   simplicity, and not as conclusive categorization, we named these observed intensity

174   fluorescence decrease signals: *deactivation responses*, as they are seemingly opposite to

175   canonical neuronal activation measured through fluorescence increase.

176   A notable example of deactivation was recorded in response to citric acid in 2 neurons

177   localized centrally in the organ in close proximity with each other. We termed these neurons

8

178   CDL1 (central-dorsal-lateral neuron 1) and CDL2, respectively. Intriguingly, CDL1 and

179   CDL2 responded to citric acid in a pattern of synchronous activation-deactivation (Fig.3A).

180   To examine into the possibility that deactivation responses were caused by top-down

181   inhibition by central interneurons, we performed recordings in animals with severed

182   connections between chemosensory neurons and CNS (Fig.3B). Detaching the brain and the

183   respective sensory nerve connections did not abolish the activation-deactivation responses

184   induced by citric acid stimulation. Likely, this pattern corresponds to ephaptic transmission

185   where the electrical field of a responding cell generates hyperpolarization in the partner cell

186   (60), also reported in the adult olfactory system (51).

187

Mapping neuronal responses across larvae shows a high level of taste multimodality

189   Next, we proceeded to match neurons based on their spatial position within the TOG organ

190   and responses recorded to individual taste series presented in figure 2A. We identified and

191   named 21 GSNs (Fig.4, y axis and 3D image). All considered responses exceeded 20% DF/F0

192   and were manually validated. Not all neurons showed the same response consistency, as

193   reflected by the stereotypy of response, meaning the percentage of times a neuron was

194   identified to respond (Fig.4A freq, grey tones with darker color denoting higher frequency).

195   Heatmap for activation and deactivation responses for each neuron were compiled separately

196   and for each cell and each tastant, we plotted the stereotypy of response next to the average

197   intensity of response (Fig.4A, x axis). Average intensities were considered only if response

198   frequencies were at least 20% for the given tastant.

199   Although deactivation responses were noted to different substances in different neurons

200   (Fig.4A, blue ovals), such events with frequency of response above 20% were only mapped to

201   CDL2 and CPV neurons, particularly for citric acid stimulation. Noteworthy, CDL1 was

202 robustly activated by citric acid while its CDL2 neighbor showed robust deactivation in

203 response to citric acid (Suppl.File2, Wilcoxon signed rank nonparametric test, p<0.05)

204 (Fig.4C), as described for their concomitant response pattern in figure 3.

205 While most GSN identities cannot be pinned down with absolute certainty, we identified the

206 AC1 neuron to likely share identity with the previously described C6 neuron, based on the

207 easily recognizable anterior position in the organ (Fig.1C & 4B) and response profiles to

208 sucrose and high salt as previously reported for C6 (48) (Fig.4D).

209 Taken together, the physiological results show an important degree of taste integration and

210 complexity – a tastant can elicit responses from multiple GSNs and a GSN can respond to

211 multiple tastants per animal or across animals, suggesting a combinatorial mode of sensory

212 encoding.

213

214 **Molecular profiles of TOG and DOG neurons at single cell resolution**

215

216 In order to assess molecular features of individual sense neurons we performed single cell

217 transcriptomic experiments on the TOG and the DOG. Due to low neuronal number and to

218 restricted access to the tissue, the choice of methodology was a limiting and important factor.

219 To generate single cells in suspension at the level of sense organs we proceeded with their

220 isolation by manual picking (Fig.5A) and importantly, we employed a deterministic DropSeq

221 approach for low cell numbers (50, 61), resulting in increased efficiency of encapsulation

222 compared to classical approaches (62, 63).

223 The single cell data was analyzed in Seurat v3.1.2 (64, 65) (Suppl.Fig.5B, see Methods),

224 obtaining a dataset of 153 cells with more than 400 genes per cell. We used UMAP

225   embedding for visualization of marker gene expression (Suppl.Fig5C) and confirmed

226   neuronal identity of the relatively homogenous cell population based on neuronal gene

227   markers (Fig.5B). Moreover, we could detect distinct and non-overlapping expression of

228   marker genes for gustatory and olfactory sensory cells. Specifically, the *Orco* gene (*Odorant*

229   *receptor co-receptor*) that is present in all olfactory neurons in the DOG (43), most probably

230   labels the olfactory neuronal population. Conversely, *proboscipedia (pb)*, a gene known to

231   mediate specification of adult mouthparts (66), shows no overlap of expression with *Orco*-

232   positive cells, labeling a distinct neuronal population (Fig.5C, left). Importantly,

233   immunofluorescence staining in embryos shows *pb* expression restricted to TOG neurons and

234   non-overlapping with *Orco* (Fig.5C, right). Furthermore, expression of the two marker genes

235   largely correlated with the two generated clusters, although less defined for *Orco*, which

236   shows a more dispersed cell expression pattern (Suppl.Fig5C).

237

238   **Chemosensory neurons display broad and narrow expression of neurotransmitter**

239   **markers**

240   To further explore molecular neurotransmitter profiles of sense neurons we performed

241   immunostainings of marker genes on distinct neuromodulator pathways. Using *Cha*-Gal4

242   (67), we found *Choline acetyltransferase (ChAT/Cha)* in virtually all sense neurons in

243   imunofluorescence staining (Fig.6A, left), corresponding to a relatively broad molecular

244   expression (Fig.6A, right). Conversely, we identified *pale (ple)* as being expressed in 2 cells

245   of the TOG as shown by TH antibody staining (Fig.6B, left), and corresponding to a cell

246   group identified in the UMAP embedding colored by expression (Fig.6B, right). *Pale* encodes

247   a tyrosine hydroxylase as the first step on dopamine synthesis pathway and is orthologous to

248   human *tyrosine hydroxylase (TH)*.

249   Other neurotransmitter markers have also shown selective molecular expression, as in the

250   case of *Vesicular glutamate transporter* (*VGlut*). Immunofluorescence on *VGlut*-Gal4 larvae

251   exposes three cells – one in the TOG, one in the DOG and a third cell in a group peripheral to

252   TOG, we named here Mec (Fig.6C). We verified the response profile of these neurons by

253   recording their physiological response to tastants introduced earlier (Fig.2A), and we

254   compared the response for each tastant with the water response. We noted sucrose responses

255   to be different than control in the TOG and the DOG neurons (Fig.6D, Suppl.File3, p<0.05,

256   Mann-Whitney test), whereas Mec cell didn't show responses distinct from water to any of

257   the tested substances. The TOG *VGlut*-positive cell did not show co-expression with C7, C2

258   or C1-Gal4 (Suppl.Fig6), its identity remaining to be determined.

259   We have detected co-expression of markers on shared neuromodulatory pathway, as in the

260   case of *Dopamine transporter (DAT)* and *Vesicular monoamine transporter (Vmat)* (Fig.7A).

261   Considering that *Cha* is expressed in all chemosensory neurons according to

262   immunofluorescence observations (Fig.6A), co-expression could be theoretically deduced

263   between this and any other neurotransmitter revealed by the molecular data. Specifically, we

264   have detected *Cha* and *DAT* co-localization in a small subset of cells as illustrated in Fig.7B.

265   Additionally, we have identified several neurotransmitter receptors linked to GABA,

266   serotonin, octopamine or dopamine signaling pathways, some of them showing co-expression

267   in certain neurons, as for example *GABA-B-R2* and the serotonergic receptor *5-HT2B*

268   (Fig.7C). Moreover, neuropeptide expression was also abundant in our data, such as

269   neuropeptide-like 2/4 precursors (*Nplp2, Nplp4*), also co-expressed with other

270   neurotransmitter markers such as *VGlut* or *Vmat* (Fig.7D & E). Co-expression of several

271   neuromodulators in numerically restricted neuronal tissues such as the TOG and DOG

272   supports the multimodal character of these sense organs but the functional implication of this

273   observation remains an open question.

274

GSNs show mechanosensory marker expression and responses

276   Mechanosensory function in the larval taste sensing was assumed to a large extent due to

277   early microscopic descriptions of chemosensory organs in *Drosophila* and in other insects (9,

278   68, 69). Although functional investigations of mechanical and chemosensory integration have

279   been explored in the adult fly (70, 71), similar studies in the larva were primarily focused on

280   food texture effects in taste behavior and learning (72, 73) while the involved

281   mechanoreceptors remain unknown. We identified expression of mechanosensory markers

282   both by means of immunofluorescence stainings and in single cell UMAP embedding (Fig.8).

283   Namely, *nanchung* (*nan*) is expressed in one TOG and one DOG cell (Fig.8A), whereas *no*

284   *mechanoreceptor potential C* (*nompC*) is present in a group of 3-4 cells of the TOG and

285   surrounding smaller sensilla (Fig.8B). We found expression of *painless* (*pain*-Gal4) by means

286   of immunolabelling in a population of up to 12 TOG cells, corresponding to a few single cells

287   in the UMAP embedding. Knowing that *pain* is involved in mechanical and thermal

288   nociception in multidendritic and chordotonal sensory neurons in the larva (74), we further

289   tested the response profiles in *pain*-expressing TOG neurons to mechanical stimulation

290   (Fig.8C).

291   To measure mechanical responses we aimed at inducing fluid shear stress on the cellular

292   membrane (75) and measuring the cell response after turning on the water flow inside the

293   microfluidic chip. As the tissue was exposed to water also during the off stimulus (in absence

294   of flow), we interpreted neuronal responses to be determined by the fluid flow and not by

295   water taste itself. We detected fluorescence intensity changes on average in 4 *pain*-Gal4 cells,

296   which were named based on their relative position and mapped to the organ. More often than

297   not, although not exclusively, we observed fluorescence intensity decrease during the on

298   stimulus, *pain*-expressing cells being potentially de-activated by shear stress (Fig.8C).

299   In a separate assay we recorded *nsyb*-Gal4 larvae for mechanosensory as well as taste sensing.

300   Interestingly, in few cases we observed neurons activated by both types of modalities, as for

301   example CM1 neuron responding to 500mM sucrose but also showing de-activation to

302   mechanical shear stress (Suppl.Fig8). This observation suggests that some GSNs could

303   integrate both mechano- and taste sensing as previously suggested (8).

304

14

Discussion

In this study we explored the physiological and molecular characteristics of *Drosophila* larval taste system. We designed an experimental framework allowing calcium imaging in all GSNs comprised by the larval primary taste-sensing organ at the periphery (the TOG, Fig.1, Suppl.Fig.1). Our approach complements previous strategies based on labeling of few single neurons or subpopulations (6, 29, 35, 39, 48), allowing for an overview of activation patterns within the organ. Strengthening our previous observations on the multimodal character of larval taste neurons (48), we identified single GSNs activated by different taste categories as well as single GSNs activated by tastants with opposite associated valence. Cell integration of different tastes might involve spatio-temporal codes, as described for gustatory discrimination in the moth (76) or combined patterns of response in cell number and type of activation. In line with our observations that one tastant elicits response in several GSNs, it is interesting to consider that the relevance of a stimulus and ultimately its behavioral output could depend on neurons firing together, concurrent activation of 2 neurons differing from their separate activation (77).

For the substances tested within this study we observed roughly a 60-70% versus 30-40% division of uni-modal versus multi-modal responding GSNs (Fig.2 & 4), comparable with tuning proportions reported for mouse fungiform taste sensing cells (78). The *best stimulus concentration* principle is arguably the strongest support of the labeled-line taste coding at the periphery in the mammalian system (79). However, this model leaves out the case of tastants activating different types of taste receptors depending on concentration as in the case of acesulfame K and saccharin, which at low concentrations activate sweet receptors but with increased concentration start activating bitter receptors (12). Accordingly, the chosen

329   substance concentrations within our assay might cause variability in response profiles, and

330   doubtlessly, modifying the dilution for the same tastants would alter the observed tuning of

331   GSNs, as shown on afferent taste neurons in mammals (15).

332   An intriguing aspect of taste physiology revealed by our observations was GCaMP

333   fluorescence decrease in GSNs, termed here *deactivation* for ease of discussion. Most notable

334   deactivation signals were recorded in CDL2 neuron and most stereotypically to citric acid

335   (Fig.3 & 4), although the phenomenon was not restricted to this neuron or tastant.

336   Interestingly, citric acid elicited concomitant activation in the neighboring cell named CDL1,

337   indicating response patterns of activation-deactivation in the CDL1-CDL2 couple, similar to

338   ephaptic signaling identified in the olfactory system of the adult fly (51). The synchronous

339   responses were not abolished when severing afferent neuronal axons (Fig.3B), implying that

340   CDL2 deactivation is not determined by a top-down inhibition from brain interneurons.

341   Additional possible explanations of the observed neuronal activity include gap junction

342   communication or tonic activity in CDL2 inhibited by citric acid stimulation, as reported in

343   sensory neurons of bumblebees and respectively in *C.elegans* (81, 82). However, the observed

344   synchronous activation coupled with deactivation responses in adjacent neurons best fit the

345   description of ephaptic signaling (60, 80), pointing towards inter-cellular communication and

346   thus emphasizing a model of signal integration in larval taste system at the periphery.

347

348   Using DisCo allowed us to successfully probe larval chemosensory organs with single cell

349   resolution (Fig.5, Suppl.Fig.5), resolving low cell input and tissue accessibility limitations.

350   We identified *pb* and *Orco* as marker genes distinctly expressed in TOG and respectively in

351   DOG neurons. If *Orco* is an olfactory co-receptor expressed in all olfactory neurons, taste

352   neuronal population is less characterized and functionally more diverse. Therefore, *pb* could

353   be an interesting candidate for further characterizing the population of *pb*-expressing GSNs.

354   Moreover, in the present work we describe distinct expression patterns of neuromodulator

355   marker genes in TOG and DOG neurons, as shown by UMAP embedding and confirmed by

356   immunostainings (Fig.6). The cholinergic profile of larval chemosensory neurons has

357   previously been reported (31, 53) but we show that some cells express glutamatergic,

358   dopaminergic and neuropeptidergic markers. Interestingly, marker genes on different

359   signaling pathways are co-expressed in subsets of cells (Fig.7), as previously demonstrated in

360   *Drosophila* CNS (54, 83). Considering the multimodal character of some larval GSNs, it

361   would be fascinating to uncover the role played by co-expression of distinct neurotransmitter

362   markers in such neurons. Nevertheless, if remains surprising that a handful of sensory neurons

363   display a diverse neurotransmitter profile, as reported here, demonstrating a large molecular

364   diversity within the neuronal sensory population.

365   Furthermore, we found expression of mechanosensory markers as revealed by UMAP

366   embedding of single-cell data and verified with immunostainings. We detected *nan* in one

367   TOG neuron and one DOG neuron, whereas *nompC* and *pain* label a larger population. We

368   recorded responses of *pain*–expressing GSNs exposed to water flow turned on and off, as we

369   intended to create fluid shear stress on the cell membrane, similarly to observations on

370   cultured cells (84) and studies on vascular tissue (85). It remains to be elucidated if shear

371   stress responses detected in *pain* neurons are mediated by Painless channel itself. Painless is a

372   protein known to be important in mechanical and thermal nociception in larvae (74), although

373   its role remains unexplored in the gustatory system. On the other hand, Painless has also been

374   shown to be involved in wasabi taste detection in adult flies in Gr66a-expressing GSNs (86)

375   and we have also found scarce co-expression between *pain* and *Gr66a* (data not shown). The

376   presence of mechanosensory neurons in the larval primary taste center has been frequently

17

377   reported (9, 49). Although chemosensory sensilla have been classically described as distinct

378   from mechanosensory sensilla (87), existence of neurons with dual chemo- and

379   mechanosensory modalities has also been implied based on their tubular dendritic body (8). In

380   our observations, some mechano-responsive neurons also show activation to gustatory cues

381   (Suppl.Fig.8), stressing on the probability of multisensory integration of taste and mechanical

382   cues.

383   Taken together, our data suggest a complex taste sensory coding in the larva, made up by

384   patterns of activity across neurons rather than by labeled individual neuronal responses for

385   discrimination between tastants. Besides canonical fluorescence increase responses we have

386   depicted fluorescence decrease signals in specific neurons pointing towards electric coupling

387   and therefore sensory cue processing at the periphery. Additionally, the neurotransmitter and

388   mechanoreceptor expression contribute to the multifaceted chemosensory system to

389   potentially explain the multimodality and multisensory character of specific taste neurons in

390   future studies.

Methods

Fly stocks.

We used the following fly strains: *nSyb*-Gal4 (gift from Shanhaz Lone), UAS-*GCaMP6m* (Bloomington #42748), UAS-*H2B*:*RFP* (gift from Boris Egger), *GMR57BO4*-Gal4 (Bl. #46355), *Gr94a*-gal4 (Bl. #57686), *Gr21a*-Gal4 (Bl. #23890), *Gr22e*-Gal4 (Bl. #57608), *Gr66a*-Gal4 (Bl. #57670), *Gr97a*-Gal4 (Bl. #57687), *Gr59e*-Gal4 (Bl. #57655), UAS:*mcd8:GFP;Or83b:RFP* (gift from Travis Carney), UAS-*myr:GFP* (Bl. #32198), *VGlut*-Gal4 (Bl. #24635) , *VGAT*-Gal4 (Bl. #58980), *Cha*-Gal4 (kindly gifted by PM Salvaterra), *nan*-Gal4 (Bl. #24903), *nompC*-Gal4 (Bl. #36361), *pain*-Gal4 (Bl. #27894), FlyFos *Orco*-GFP (VDRC 318654).

Immunostainings.

3rd instar larvae (4 days after egg laying) were washed and dissected in ice-cold PBS. Tissue containing chemosensory neurons was fixed in 3,7% formaldehyde for 18-20min at room temperature. After fixation, incubation in primary antibodies was performed at 4°C overnight, then in secondary antibodies at 4°C overnight, and finally, in Vectashield antifade medium (Vector Laboratories) for at least 1h before mounting the samples on microscope slides. After each step described above, PBST (PBS 0,3% Triton X-100) was employed for three consecutive plus three 30-minute washes at room temperature.

Immunolabelling against Pb (Fig.5C) was performed at embryonic stage. Embryos were washed in tap water and placed in a plastic mesh in a sampling manifold. (Millipore XX2702550). First, they were dechorionated in 2.5% sodium hypochlorite (household bleach)

414   for 2 minutes. Embryos were then fixed in a 1:1 solution of n-heptane:PEM buffer with 3.7%

415   formaldehyde for 20 minutes at room temperature on a rotating wheel. Upon fixation,

416   embryos were washed with methanol and blocked for 1 hour at room temperature with 5%

417   normal goat serum in PBST. The samples were incubated with antibodies and mounted as

418   described above.

419   Confocal images were acquired on a Leica TCS SPE-5 confocal, using the 40x oil immersion

420   objective for larval staining and the 63X glycerol immersion for embryo staining, at 0.8-1um

421   slice thickness. Images were assembled using Fiji (88) and Adobe Illustrator.

422   Primary antibodies: chicken anti-GFP (1:1000, Abcam, ab13970), rabbit anti-DsRed (1:1000,

423   Clontech, No. 632496), rat anti-ELAV (1:30, No. 7E8A10), anti-TH (1:100, Millipore,

424   ab_390204), rabbit anti-Pb 1:100 (gift of Thomas Kaufman, Cribbs, 1992 #475). Secondary

425   antibodies conjugated with Alexa Fluor fluorescent proteins (488, 568, 647) were used in

426   dilution of 1:200 (Molecular Probes no. A-11008, A-11039, A-21244, A-21247, A-11011).

427

428   **Chemicals**.

429   For calcium imaging experiments the highest purity available was chosen for all chemicals

430   used in this study: L-Alanine (Sigma-Aldrich, 56-41-7), L-Glutamine (Sigma-Aldrich, 56-85-

431   9), L-Aspartic acid (Sigma-Aldrich, 56-84-8), L-Glutamic acid (Sigma-Aldrich, 56-86-0), L-

432   Asparagine (Sigma-Aldrich, 70-47-3), L-Proline (Sigma-Aldrich, 147-85-3), L-Tyrosine

433   (Sigma-Aldrich, 60-17-4), L-Threonine (Sigma-Aldrich, 72-19-5), L-Phenylalanine (Sigma-

434   Aldrich, 63-91-2), L-Lysine (Sigma-Aldrich, 56-87-1), L-Arginine (Sigma-Aldrich, 74-79-3),

435   L-Histidine (Sigma-Aldrich, 71-00-1), L-Serine (Sigma-Aldrich, 56-45-1), L-Valine (Sigma-

436   Aldrich, 72-18-4), L-Cysteine (Sigma-Aldrich, 52-90-4), L-Methionine (Sigma-Aldrich, 63-

437   68-3), L-Leucine (Sigma-Aldrich, 61-90-5), L-Isoleucine (Sigma-Aldrich, 73-32-5), L-

438   Tryptophan (Sigma-Aldrich, 73-22-3), L-Glycine (Roth, 3187.3), D-Sucrose (Sigma-Aldrich,

439   57-50-1), D-Glucose (Sigma-Aldrich, 50-99-7), G-Fructose (Fluka, 57-48-7), D-Trehalose

440   dihydrate (Roth, 9286.1), D-Arabinose (Sigma-Aldrich, 10323-20-3), D-Maltose

441   monohydrate (Sigma-Aldrich, 6363-53-7), D-Mannose (Sigma-Aldrich, 3458-28-4), D-

442   Galactose (Roth, 4979.1), D-Cellobiose (Roth, 6840.3), Lactose monohydrate (Roth, 8921.1),

443   Quinine hemisulfate salt monohydrate (Sigma-Aldrich, 6119-70-6), Denatonium benzoate

444   (Aldrich, 3734-33-6), Caffeine anhydrous (Fluka, 58-08-2), Coumarin (Sigma-Aldrich, 91-

445   64-5), Sucrose octaacetate (Aldrich, 126-17-7), Lobeline hydrochloride (Aldrich, 134-63-4),

446   Theophyline (Sigma-Aldrich, 58-55-9), Strychnine (Roth, 4843.1), Potassium chloride

447   (Merck, 7447-40-7), Sodium chloride (Sigma-Aldrich, 7647-14-5), Citric acid (Sigma-

448   Aldrich, 77-92-9).

449   **Chemicals used in cell dissociation experiments**: elastase (Sigma-Aldrich, E0258),

450   collagenase (Sigma-Aldrich, C9722), PBS (Thermo Fisher Scientific, AM9624), BSA

451   (Thermo Fisher Scientific, AM2616), Murine inhibitor (New England Biolabs (NEB,

452   M0314L).

453

454   **Calcium imaging.**

455   The semi-intact sample for calcium-imaging recordings was prepared as previously described

456   (57). 3rd instar larval heads comprising chemosensory neurons, the brain and the connecting

457   nerves were dissected in AHL (adult hemolymph like) saline solution. The tissue was

458   introduced into the microfluidic chip and the sample was connected to the tubing and

459   micropump setup. For whole organ TOG recordings UAS-*GCaMP6m* (55) was used to

460   genetically label all neurons and *RFP* was expressed in nuclei using UAS-*H2B:RFP* (56).

461   Stacks were set to 15 slices of 1,5 μm thickness each, pixel binning of 2, with resulting time

462   acquisition speed of 0.5 stacks (time-points) per second. For recordings from *VGlut*-Gal4

463   neurons, we used the same UAS reporter lines to image the three neurons belonging to the

464   TOG and the DOG, but due to a deeper tissue extending over both organs, we set the stacks to

465   25 slices of 2,5 μm thickness each, preserving the time acquisition speed.

466   The microscope of choice was a spinning-disk confocal Visitron CSU-W1. Recordings were

467   exported as .nd files and further processed in Fiji/ImageJ and Imaris software. For each

468   recording an RFP stack was acquired prior to the CGaMP time-series.

469   **Taste Stimulation.** Each tastant was administered using a micropump (mp6, Bartels

470   Mikrotechnik) controlled in VisiView software through built-in macros. Millipore water was

471   used as solvent for taste solutions and as washing control. For each taste stimulation macros

472   were designed for 2-minute recordings to allow 1 minute pre-wash followed by 30-second

473   stimulation and a final 30-second wash.

474   **Taste stimulation with series of individual tastants.** The sequence of chemicals within a

475   trial was randomized. We used two series of tastants (Suppl.Table 1), each containing 5

476   substances from 5 different taste categories. Series 1 consisted of sucrose (sweet), denatonium

477   (bitter), NaCl 1M (high salt), valine (amino acid) and citric acid (sour). Series 2 consisted of

478   sucrose, quinine (bitter), NaCl 100mM (low salt), arginine (amino acid) and citric acid. Each

479   recorded animal was stimulated with all the tastants within one series. A total of 15 TOG

480   organs were recorded, 7 for series 1 and 8 for series 2.

481   **Taste stimulation with groups of tastants.** We compiled 2 groups of sugars, each containing

482   5 sugars at a concentration of 100 mM each: monosaccharides (fructose, glucose, arabinose,

483   mannose, galactose), and disaccharides (sucrose, trehalose, maltose, lactose, cellobiose).

484   Amino acids were prepared in 4 groups (A, B, C and D) as previously described by Park et al.

485   (59) (Suppl.Table 1). Tyrosine was included in group B at a concentration of 1mM. Salt taste

486   groups contained NaCl and KCl in equal proportions at a total concentration of 50mM (low

487   salt) and respectively 1M (high salt). Bitter tastants were randomized in 2 groups of 4

488   substances each, with a final concentration of 22mM and respectively 13mM, restricted by the

489   solubility of certain substances such as lobeline or strychnine reduced to 1mM instead of

490   10mM (Suppl.Table 1): DSoTC group (denatonium benzoate, sucrose octaacetate,

491   theophylline, coumarin), and respectively QLSC group (quinine, lobeline, strychnine,

492   caffeine).

493   **Mechanical stimulation.** Macros were adjusted to switch water flow between on and off at

494   30-second interval. The sample was exposed to water in both conditions; therefore,

495   corresponding neuronal responses were interpreted to be result of shear stress mechanical

496   stimulation (75) and not caused by water taste.

497

498   **Data processing and analysis of whole-organ physiological recordings.**

499   We first carried out deconvolution processing on Huygens platform of RFP stacks and

500   GCaMP recordings. A Fiji/ImageJ plugin was written to duplicate the RFP signal onto all

501   time-points of the CGaMP recording (Suppl.Fig.1A). If the animal movement was

502   considerable, a 3D drift correction was applied on the GFP signal before merging the two

503   channels. Eventual misalignment between the two signals (caused by drifts or animal

504   movement) was corrected by writing a Fiji/ImageJ macro for manually guided realignment

505   (Suppl.Fig.1B). A final 3D drift correction (89) was then performed for better stabilization.

506   The recording was transferred in Imaris for automatic segmentation with spots of 3,5um

507   diameter. Each uniquely identified neuron though spot detection received an identity and a

508   corresponding fluorescence trace over time (Suppl.Fig.1C). An extra spot was created in

23

509   proximity to the organ, serving as background fluorescence to be subtracted from all cell

510   spots. Signal processing and downstream analysis were performed with R (90, 91).

511   Normalization of fluorescence values followed the formula $(F_t-F0)/F0$, F_t being the intensity

512   at timepoint t and F0 the baseline as average intensity of 10 frames prior stimulation.

513   Response amplitude was calculated as the difference between the peak intensity after

514   stimulation (average of 5 frames near the maximal fluorescence value) and F0. All traces were

515   individually inspected to exclude false positive responses. Responses were considered for

516   further analysis if their amplitude was minimum 20% DF/F0. To calculate taste integration

517   percentages (Fig.2), for each a specific dataset we selected all responding neurons and then

518   determined the fraction of neurons activated by one or by multiple tastants / taste groups per

519   animal. Illustrative lists of responding neurons as well as number of neurons and responses

520   considered for analysis within each test category were assembled in Supplementary File 1.

521   Neurons responding to individual tastants were mapped across organs (Fig.4) by manually

522   assessing their relative position and physiological response. Supplementary File 2 contains he

523   activation or deactivation values with frequencies of response above 20% for mapped neurons

524   and the corresponding Wilcoxon signed rank nonparametric test p-values. Figures were

525   generated in RStudio (92) using "ggplot2", "reshape2" and "scales" packages (93-95) or in

526   GraphPad Prism 7 and adjusted in Adobe Illustrator.

527   **Calcium imaging analysis of *VGlut*-positive cells.** For recordings of *VGlut*-Gal4 neurons,

528   analysis was entirely performed in Fiji/ImageJ. Cell segmentation was replaced by setting

529   regions of interest (ROI) around each of the 3 somas and fluorescence intensity over time was

530   extracted after applying a z-projection of the stack recordings. Normalization was performed

531   as above and all taste responses were compared to water response for each neuron. Response

532   values and Mann-Whitney tests of comparisons with control were compiled in Supplementary

533   File 3. Analysis and figures were generated in GraphPad Prism 7.

534

Single-cell chemosensory cell suspension preparation for DisCo.

3rd instar larvae of genotype *nsyb*-Gal4 > UAS-*mcd8:GFP; Or83b:RFP* were collected from food, washed in tap water, PBS, dropped in ethanol and again PBS and dissected in ice-cold PBS in such a manner that only the external chemosensory organs were kept, avoiding to include also the pharyngeal tissue containing internal chemosensory organs. The isolated material was then placed on ice in elastase 1 mg/ml in siliconized 2-ml tubes. After dissecting 20-30 larvae (20-25 minutes), the tube sample was placed at room temperature to initiate digestion. After 30 minutes the tissues was washed in PBS+BSA0,05% and dissociated by up-down pipetting for 120 times using siliconized 200p pipette tips. Separated TOG and DOG organs were detected using a fluorescence stereomicroscope and manually picked with a glass micropipette, placed in a final dissociation enzyme mix of Collagenase 1mg/ml + Elastase 0,5mg/ml for 10-15 minutes for single cell suspension. The reaction was stopped with PBS + BSA 0,05%. Murine inhibitor was added at each step of the dissociation protocol.

Deterministic co-encapsulation (DisCo) of chemosensory neurons for single cell transcriptomics.

Microfluidic chip design, fabrication and device handling are described elsewhere (50). Following organ dissociation, target cell suspension was diluted in the cell loading buffer containing PBS 0.01 % BSA (Sigma B8667), 6% Optiprep (Sigma D1556) and Murine RNase inhibitor (NEB M0314L) in the loading tip connected to the DisCo chip. After bead-cell in droplet co-encapsulation, sample droplets were transferred to a bead collection chip. Subsequently to bead capture, washing, reverse transcription (Thermo Scientific EP0753) and Exonuclease I (NEB M0293L) reactions were performed on-chip (61). Beads containing cDNA were then eluted and cDNA was amplified for 21 cycles using Kapa HiFi Hot start

558   ready mix (Roche #07958935001). Amplified cDNA was then purified (GC biotech CPCR-

559   0050) for quality assessment with Fragment Analyzer (Agilent). Libraries were then

560   tagmented using in-house Tn5 (96), size selected and purified for sequencing on NextSeq 500

561   system (Illumina) following recommendations from original Drop-seq protocol (97) (20 bp

562   for read 1 and 50 bp for read2) at sequencing depth above 400.000 reads per cell.

563   **Single-cell data pre-processing and analysis.** The data analysis was performed using the

564   Drop-seq tools package (62). After pre-processing, reads were aligned to *Drosophila*

565   *melanogaster* reference genome (Ensembl version 86) using STAR (version 2.7.0.e) (98).

566   Following the alignment, BAM files were processed using the initial package and read-count

567   matrices were generated.

568   Downstream analysis was done using the Seurat package (65) version 3.1.2 in RStudio.

569   Individual data sets were loaded and used to create separate normalized and scaled Seurat

570   objects of minimum 400 genes per cell. In order to apply unique cell filters we merged the

571   data and then excluded cells with high gene number and high UMIs as potential doublets and

572   cells with high mitochondrial gene percentage indicating potential apoptotic cells. Due to

573   observed correlation between cells with high gene number (nGene, Suppl.Fig.5B) and cells

574   with high UMIs (nCount, Suppl.Fig.5B), by applying UMI threshold at 50000 we also

575   eliminated cells with more than 4000 genes. Cells with mitochondrial gene percentage under

576   9% were kept for further analysis (Suppl.Fig.5B). Data was then integrated to circumvent

577   batch effects using Seurat functions *FindIntegrationAnchors* and *IntegrateData*. As we were

578   interested in characterizing neurons, we used the *subset* function to keep only cells expressing

579   *nSyb* or *peb* neuronal markers, excluding eventual surrounding tissue or cuticle cells. On the

580   final dataset of 153 neurons PCA (principal component analysis) computation was followed

581   by UMAP embedding and clustering (Suppl.Fig.5C) was performed at 0.5 resolution.

References

1.   Gerber B, Stocker RF. The *Drosophila* larva as a model for studying chemosensation and chemosensory learning: a review. Chemical senses. 2007;32(1):65-89.

2.   El-Keredy A, Schleyer M, Konig C, Ekim A, Gerber B. Behavioural analyses of quinine processing in choice, feeding and learning of larval Drosophila. PLoS One. 2012;7(7):e40525.

3.   Konig C, Schleyer M, Leibiger J, El-Keredy A, Gerber B. Bitter-sweet processing in larval *Drosophila*. Chem Senses. 2014;39(6):489-505.

4.   Kim H, Choi MS, Kang K, Kwon JY. Behavioral Analysis of Bitter Taste Perception in Drosophila Larvae. Chem Senses. 2016;41(1):85-94.

5.   Schipanski A, Yarali A, Niewalda T, Gerber B. Behavioral analyses of sugar processing in choice, feeding, and learning in larval Drosophila. Chem Senses. 2008;33(6):563-73.

6.   Croset V, Schleyer M, Arguello JR, Gerber B, Benton R. A molecular and neuronal basis for amino acid sensing in the Drosophila larva. Sci Rep. 2016;6:34871.

7.   Kudow N, Miura D, Schleyer M, Toshima N, Gerber B, Tanimura T. Preference for and learning of amino acids in larval Drosophila. Biol Open. 2017;6(3):365-9.

8.   Stocker RF. The organization of the chemosensory system in *Drosophila melanogaster*: a review. Cell and tissue research. 1994;275(1):3-26.

9.   Stocker RF. Design of the larval chemosensory system. Adv Exp Med Biol. 2008;628:69-81.

10.   Chandrashekar J, Hoon MA, Ryba NJ, Zuker CS. The receptors and cells for mammalian taste. Nature. 2006;444(7117):288-94.

11.   Huang AL, Chen XK, Hoon MA, Chandrashekar J, Guo W, Trankner D, et al. The cells and logic for mammalian sour taste detection. Nature. 2006;442(7105):934-8.

12.   Yarmolinsky DA, Zuker CS, Ryba NJ. Common sense about taste: from mammals to insects. Cell. 2009;139(2):234-44.

13.   Barretto RPJ, Gillis-Smith S, Chandrashekar J, Yarmolinsky DA, Schnitzer MJ, Ryba NJP, et al. The neural representation of taste quality at the periphery. Nature. 2015;517(7534):373-U511.

14.   Smith DV, St John SJ. Neural coding of gustatory information. Curr Opin Neurobiol. 1999;9(4):427-35.

15.   Wu A, Dvoryanchikov G, Pereira E, Chaudhari N, Roper SD. Breadth of tuning in taste afferent neurons varies with stimulus strength. Nature Communications. 2015;6.

16.   Tomchik SM, Berg S, Kim JW, Chaudhari N, Roper SD. Breadth of tuning and taste coding in mammalian taste buds. Journal of Neuroscience. 2007;27(40):10840-8.

17.   Chaudhari N, Roper SD. The cell biology of taste. J Cell Biol. 2010;190(3):285-96.

18.   Dahanukar A, Lei YT, Kwon JY, Carlson JR. Two Gr genes underlie sugar reception in Drosophila. Neuron. 2007;56(3):503-16.

19.   Fujii S, Yavuz A, Slone J, Jagge C, Song X, Amrein H. *Drosophila* Sugar Receptors in Sweet Taste Perception, Olfaction, and Internal Nutrient Sensing. Curr Biol. 2015.

20.   Thorne N, Chromey C, Bray S, Amrein H. Taste perception and coding in Drosophila. Curr Biol. 2004;14(12):1065-79.

21.   Liman ER, Zhang YV, Montell C. Peripheral coding of taste. Neuron. 2014;81(5):984-1000.

22.   French A, Ali Agha M, Mitra A, Yanagawa A, Sellier MJ, Marion-Poll F. Drosophila Bitter Taste(s). Front Integr Neurosci. 2015;9:58.

23.   Zhang YV, Ni J, Montell C. The molecular basis for attractive salt-taste coding in Drosophila. Science. 2013;340(6138):1334-8.

24.   Hussain A, Zhang M, Ucpunar HK, Svensson T, Quillery E, Gompel N, et al. Ionotropic Chemosensory Receptors Mediate the Taste and Smell of Polyamines. Plos Biology. 2016;14(5).

25.   Lee MJ, Sung HY, Jo H, Kim HW, Choi MS, Kwon JY, et al. Ionotropic Receptor 76b Is Required for Gustatory Aversion to Excessive Na+ in Drosophila. Mol Cells. 2017;40(10):787-95.

26.   Tauber JM, Brown EB, Li Y, Yurgel ME, Masek P, Keene AC. A subset of sweet-sensing neurons identified by IR56d are necessary and sufficient for fatty acid taste. PLoS Genet. 2017;13(11):e1007059.

27.   Ahn JE, Chen Y, Amrein H. Molecular basis of fatty acid taste in Drosophila. Elife. 2017;6.

28.   Ganguly A, Pang L, Duong VK, Lee A, Schoniger H, Varady E, et al. A Molecular and Cellular Context-Dependent Role for Ir76b in Detection of Amino Acid Taste. Cell Rep. 2017;18(3):737-50.

29.   Sanchez-Alcaniz JA, Silbering AF, Croset V, Zappia G, Sivasubramaniam AK, Abuin L, et al. An expression atlas of variant ionotropic glutamate receptors identifies a molecular basis of carbonation sensing. Nat Commun. 2018;9(1):4252.

30.   Jaeger AH, Stanley M, Weiss ZF, Musso PY, Chan RC, Zhang H, et al. A complex peripheral code for salt taste in Drosophila. Elife. 2018;7.

31.   Vosshall LB, Stocker RF. Molecular architecture of smell and taste in *Drosophila*. Annual review of neuroscience. 2007;30:505-33.

32.   Scott K, Brady R, Jr., Cravchik A, Morozov P, Rzhetsky A, Zuker C, et al. A chemosensory gene family encoding candidate gustatory and olfactory receptors in *Drosophila*. Cell. 2001;104(5):661-73.

33.   Colomb J, Grillenzoni N, Ramaekers A, Stocker RF. Architecture of the primary taste center of *Drosophila* melanogaster larvae. The Journal of comparative neurology. 2007;502(5):834-47.

34.   Rimal S, Lee Y. The multidimensional ionotropic receptors of Drosophila melanogaster. Insect Mol Biol. 2018;27(1):1-7.

35.   Stewart S, Koh TW, Ghosh AC, Carlson JR. Candidate ionotropic taste receptors in the *Drosophila* larva. Proc Natl Acad Sci U S A. 2015.

36.   Alves G, Salle J, Chaudy S, Dupas S, Maniere G. High-NaCl perception in *Drosophila* melanogaster. J Neurosci. 2014;34(33):10884-91.

37.   Mast JD, De Moraes CM, Alborn HT, Lavis LD, Stern DL. Evolved differences in larval social behavior mediated by novel pheromones. Elife. 2014;3:e04205.

38. Xu J, Sornborger AT, Lee JK, Shen P. Drosophila TRPA channel modulates sugar-stimulated neural excitation, avoidance and social response. Nat Neurosci. 2008;11(6):676-82.

39. Kwon JY, Dahanukar A, Weiss LA, Carlson JR. Molecular and cellular organization of the taste system in the *Drosophila* larva. The Journal of neuroscience : the official journal of the Society for Neuroscience. 2011;31(43):15300-9.

40. Apostolopoulou AA, Rist A, Thum AS. Taste processing in *Drosophila* larvae. frontiers in integrative Neuroscience. 2015;9.

41. Python F, Stocker RF. Adult-like complexity of the larval antennal lobe of D. melanogaster despite markedly low numbers of odorant receptor neurons. J Comp Neurol. 2002;445(4):374-87.

42. Gendre N, Luer K, Friche S, Grillenzoni N, Ramaekers A, Technau GM, et al. Integration of complex larval chemosensory organs into the adult nervous system of *Drosophila*. Development. 2004;131(1):83-92.

43. Larsson MC, Domingos AI, Jones WD, Chiappe ME, Amrein H, Vosshall LB. Or83b encodes a broadly expressed odorant receptor essential for *Drosophila* olfaction. Neuron. 2004;43(5):703-14.

44. Kreher SA, Kwon JY, Carlson JR. The molecular basis of odor coding in the *Drosophila* larva. Neuron. 2005;46(3):445-56.

45. Fishilevich E, Domingos AI, Asahina K, Naef F, Vosshall LB, Louis M. Chemotaxis behavior mediated by single larval olfactory neurons in *Drosophila*. Current biology : CB. 2005;15(23):2086-96.

46. Mathew D, Martelli C, Kelley-Swift E, Brusalis C, Gershow M, Samuel AD, et al. Functional diversity among sensory receptors in a Drosophila olfactory circuit. Proc Natl Acad Sci U S A. 2013;110(23):E2134-43.

47. Si G, Kanwal JK, Hu Y, Tabone CJ, Baron J, Berck M, et al. Structured Odorant Response Patterns across a Complete Olfactory Receptor Neuron Population. Neuron. 2019;101(5):950-62 e7.

48. van Giesen L, Hernandez-Nunez L, Delasoie-Baranek S, Colombo M, Renaud P, Bruggmann R, et al. Multimodal stimulus coding by a gustatory sensory neuron in Drosophila larvae. Nat Commun. 2016;7:10687.

49. Rist A, Thum AS. A map of sensilla and neurons in the taste system of drosophila larvae. J Comp Neurol. 2017;525(18):3865-89.

50. Bues J, Biočanin M, Pezoldt J, Dainese R, Chrisnandy A, Rezakhani S, et al. Deterministic scRNA-seq of individual intestinal organoids reveals new subtypes and coexisting distinct stem cell pools. BioRxiv. 2020.

51. Su CY, Menuz K, Reisert J, Carlson JR. Non-synaptic inhibition between grouped neurons in an olfactory circuit. Nature. 2012;492(7427):66-71.

52. Zhang Y, Tsang TK, Bushong EA, Chu LA, Chiang AS, Ellisman MH, et al. Asymmetric ephaptic inhibition between compartmentalized olfactory receptor neurons. Nat Commun. 2019;10(1):1560.

53. Python F, Stocker RF. Immunoreactivity against choline acetyltransferase, gamma-aminobutyric acid, histamine, octopamine, and serotonin in the larval chemosensory system of Dosophila melanogaster. J Comp Neurol. 2002;453(2):157-67.

54. Brunet Avalos C, Maier GL, Bruggmann R, Sprecher SG. Single cell transcriptome atlas of the Drosophila larval brain. Elife. 2019;8.

55. Chen TW, Wardill TJ, Sun Y, Pulver SR, Renninger SL, Baohan A, et al. Ultrasensitive fluorescent proteins for imaging neuronal activity. Nature. 2013;499(7458):295-300.

56. Egger B, Boone JQ, Stevens NR, Brand AH, Doe CQ. Regulation of spindle orientation and neural stem cell fate in the Drosophila optic lobe. Neural Dev. 2007;2:1.

57. van Giesen L, Neagu-Maier GL, Kwon JY, Sprecher SG. A microfluidics-based method for measuring neuronal activity in Drosophila chemosensory neurons. Nat Protoc. 2016;11(12):2389-400.

58. Marella S, Fischler W, Kong P, Asgarian S, Rueckert E, Scott K. Imaging taste responses in the fly brain reveals a functional map of taste category and behavior. Neuron. 2006;49(2):285-95.

59. Park J, Carlson JR. Physiological responses of the Drosophila labellum to amino acids. J Neurogenet. 2018;32(1):27-36.

60. Faber DS, Pereda AE. Two Forms of Electrical Transmission Between Neurons. Front Mol Neurosci. 2018;11:427.

61. Biocanin M, Bues J, Dainese R, Amstad E, Deplancke B. Simplified Drop-seq workflow with minimized bead loss using a bead capture and processing microfluidic chip. Lab Chip. 2019;19(9):1610-20.

62. Macosko EZ, Basu A, Satija R, Nemesh J, Shekhar K, Goldman M, et al. Highly Parallel Genome-wide Expression Profiling of Individual Cells Using Nanoliter Droplets. Cell. 2015;161(5):1202-14.

63. Klein AM, Macosko E. InDrops and Drop-seq technologies for single-cell sequencing. Lab Chip. 2017;17(15):2540-1.

64. Satija R, Farrell JA, Gennert D, Schier AF, Regev A. Spatial reconstruction of single-cell gene expression data. Nat Biotechnol. 2015;33(5):495-502.

65. Stuart T, Butler A, Hoffman P, Hafemeister C, Papalexi E, Mauck WM, 3rd, et al. Comprehensive Integration of Single-Cell Data. Cell. 2019;177(7):1888-902 e21.

66. Rusch DB, Kaufman TC. Regulation of proboscipedia in Drosophila by homeotic selector genes. Genetics. 2000;156(1):183-94.

67. Salvaterra PM, Kitamoto T. Drosophila cholinergic neurons and processes visualized with Gal4/UAS-GFP. Brain Res Gene Expr Patterns. 2001;1(1):73-82.

68. Stocker RF. The Organization of the Chemosensory System in Drosophila-Melanogaster - a Review. Cell and Tissue Research. 1994;275(1):3-26.

69. Chu-Wang IW, Axtell RC. Fine structure of the terminal organ of the house fly larva, Musca domestica L. Z Zellforsch Mikrosk Anat. 1972;127(3):287-305.

70. Jeong YT, Oh SM, Shim J, Seo JT, Kwon JY, Moon SJ. Mechanosensory neurons control sweet sensing in Drosophila. Nat Commun. 2016;7:12872.

71. Sanchez-Alcaniz JA, Zappia G, Marion-Poll F, Benton R. A mechanosensory receptor required for food texture detection in Drosophila. Nat Commun. 2017;8:14192.

72. Apostolopoulou AA, Hersperger F, Mazija L, Widmann A, Wust A, Thum AS. Composition of agarose substrate affects behavioral output of *Drosophila* larvae. Frontiers in behavioral neuroscience. 2014;8:11.

73. Kudow N, Kamikouchi A, Tanimura T. Softness sensing and learning in Drosophila larvae. J Exp Biol. 2019;222(Pt 7).

74. Tracey WD, Jr., Wilson RI, Laurent G, Benzer S. painless, a Drosophila gene essential for nociception. Cell. 2003;113(2):261-73.

75. Brown TD. Techniques for mechanical stimulation of cells in vitro: a review. J Biomech. 2000;33(1):3-14.

76. Reiter S, Campillo Rodriguez C, Sun K, Stopfer M. Spatiotemporal Coding of Individual Chemicals by the Gustatory System. J Neurosci. 2015;35(35):12309-21.

77. Hernandez-Nunez L, Belina J, Klein M, Si G, Claus L, Carlson JR, et al. Reverse-correlation analysis of navigation dynamics in larva using optogenetics. Elife. 2015;4.

78. Jisoo Han MC. Comprehensive functional screening of taste sensation in vivo. bioRxiv. 2018.

79. Smith DV, Travers JB. Metric for the Breadth of Tuning of Gustatory Neurons. Chemical Senses & Flavour. 1979;4(3):215-29.

80. Jefferys JG. Nonsynaptic modulation of neuronal activity in the brain: electric currents and extracellular ions. Physiol Rev. 1995;75(4):689-723.

81. Miriyala A, Kessler S, Rind FC, Wright GA. Burst Firing in Bee Gustatory Neurons Prevents Adaptation. Curr Biol. 2018;28(10):1585-94 e3.

82. Saro G, Lia AS, Thapliyal S, Marques F, Busch KE, Glauser DA. Specific Ion Channels Control Sensory Gain, Sensitivity, and Kinetics in a Tonic Thermonociceptor. Cell Rep. 2020;30(2):397-408 e4.

83. Meissner GW, Nern A, Singer RH, Wong AM, Malkesman O, Long X. Mapping Neurotransmitter Identity in the Whole-Mount Drosophila Brain Using Multiplex High-Throughput Fluorescence in Situ Hybridization. Genetics. 2019;211(2):473-82.

84. Xu Y, Qin S, Niu Y, Gong T, Zhang Z, Fu Y. Effect of fluid shear stress on the internalization of kidney-targeted delivery systems in renal tubular epithelial cells. Acta Pharm Sin B. 2020;10(4):680-92.

85. White CR, Frangos JA. The shear stress of it all: the cell membrane and mechanochemical transduction. Philos Trans R Soc Lond B Biol Sci. 2007;362(1484):1459-67.

86. Al-Anzi B, Tracey WD, Jr., Benzer S. Response of Drosophila to wasabi is mediated by painless, the fly homolog of mammalian TRPA1/ANKTM1. Curr Biol. 2006;16(10):1034-40.

87. Singh RN, Singh K. Fine-Structure of the Sensory Organs of *Drosophila-Melanogaster* Meigen Larva (Diptera, Drosophilidae). International Journal of Insect Morphology & Embryology. 1984;13(4):255-73.

88. Schindelin J, Arganda-Carreras I, Frise E, Kaynig V, Longair M, Pietzsch T, et al. Fiji: an open-source platform for biological-image analysis. Nat Methods. 2012;9(7):676-82.

89. Parslow A, Cardona A, Bryson-Richardson RJ. Sample drift correction following 4D confocal time-lapse imaging. J Vis Exp. 2014(86).

90. Team RC. R: A language and environment for statistical computing. R Foundation for Statistical Computing, Vienna, Austria. URL https://www.R-project.org/. 2017.

91. Wickham H. FR, Henry L. and Müller K. dplyr: A Grammar of Data Manipulation. R package version 0.7.6. https://CRAN.R-project.org/package=dplyr. 2018.

799   92.   Team R. RStudio: Integrated Development for R. 2015.

800   93.   Wickham H. Reshaping Data with the reshape Package. Journal of Statistical
801   Software. 2007;21(12):1-20.

802   94.   Wickham H. ggplot2: Elegant Graphics for Data Analysis. 2009.

803   95.   Wickham H. SD, RStudio. scales: Scale Functions for Visualization. 2019.

804   96.   Picelli S, Bjorklund AK, Reinius B, Sagasser S, Winberg G, Sandberg R. Tn5
805   transposase and tagmentation procedures for massively scaled sequencing projects. Genome
806   Res. 2014;24(12):2033-40.

807   97.   Macosko E.Z. GM, McCarroll S.A. Drop-Seq Laboratory Protocol version 3.1. 2015.

808   98.   Dobin A, Davis CA, Schlesinger F, Drenkow J, Zaleski C, Jha S, et al. STAR:
809   ultrafast universal RNA-seq aligner. Bioinformatics. 2013;29(1):15-21.

810

Acknowledgements

We thank the Sprecher lab for support and useful discussions and Joern Pezoldt, Wanze Chen and Maria Litovchenko from Deplancke lab for support, valuable comments and practical advice. We thank EPFL's Gene Expression Core Facility for sequencing support and Rommelaere Samuel from Lemaitre lab for providing fluorescent microscope during single-cell preparation experiments. We are also grateful to Boris Egger for guidance on microscopy and data analysis and to everyone who shared with us fly stocks and reagents.

Author contributions

GLM and SGS designed the study and wrote the paper. GLM performed physiological recordings, immunostainings, and single cell dissociation, analyzed the data and created the figures. MB and JB performed DisCo experiments and library preparation. FM wrote the plugins and macros necessary for calcium imaging data processing and assisted in establishing the analysis pipeline. CBA identified and determined *proboscipedia* immunofluorescence expression and assisted with single cell sequencing analysis in Seurat. BD, JYK and SGS assisted in interpretation of results.

Additional information. The authors declare no competing interests.

Data Availability

Single cell RNAseq data reported in this study are available on NCBI GEO; accession number GSE149975.

832   Fiji/ImageJ plugin and macro for calcium imaging data processing are available as

833   supplementary file.

834   Data generated and analyzed within the present study are available from the corresponding

835   author upon request.

836

837 **Figure 1: Peripheral taste neurons of the fruit fly larva – visualization and calcium**

838 **imaging.**

839 A. The chemosensory system of the larva. External sense organs extend dendrites to the

840 periphery and have main olfactory function – the DOG (dorsal organ ganglion), or

841 gustatory function – the TOG (terminal organ ganglion) and the VOG (ventral organ

842 ganglion). Dendrites of the internal dorsal, ventral and posterior pharyngeal sense organs

843 (DPS, VPS and PPS) innervate the pharynx, thus involved in taste sensing during food

844 ingestion. All chemosensory neurons project axons to the brain in the subesophageal

845 ganglion (SOG) – first central taste integration relay – or to the antennal lobe (AL) for

846 central olfactory processing. Adapted from (1).

847 B. External chemosensory organs. 7 GSNs previously identified and named C1-C7 are

848 represented here by the color code they were first described with (39, 48). Used Gal4

849 lines: *Gr22e*-Gal4 (C1), *Gr94a*-Gal4 (C2), *Gr59d*-Gal4 (C1, C2, C4), *Gr66a*-Gal4 (C1,

850 C2, C3, C4), *Gr59e*-Gal4 (C5), *Gr21a*-Gal4 (C6), *GMR57BO4*-Gal4 (C7).

851 C. UAS-*myrGFP* reporter was expressed in individual GSNs using corresponding Gal4 lines

852 (B). We observed a relatively stereotypic position of specific neurons within the organ

853 across animals (n ≥ 3) – exemplified on C6 and C1.

854 D. Illustrative 3D map of TOG segmented cells. Position of neurons with known identities

855 (white dots) is approximated based on separate immunostainings.

856 E. Representative recording of the larval primary taste organ stimulated with citric acid

857 100mM. Cytoplasmic expression of *GCaMP6m* and nuclear expression of *RFP* in all

858 neurons (upper left panel) and cell segmentation (white spots, lower left panel).

859 Responding neurons are indicated by blue, red and magenta arrows (upper right panel)

860 and by dots and corresponding fluorescence traces of same colors (lower right panels).

861

Supplementary Figure 1: Whole organ calcium imaging – data processing.

A. The RFP nuclear signal acquired as a single stack was duplicated to all timepoints of the GCaMP time-series using an in-house written plugin. Step performed in Fiji/ImageJ.

B. On the recording comprising both fluorescence channels, any misalignment between the two signals due to animal movement or slight drift was corrected through a manually assisted macro. Step performed in Fiji/ImageJ.

C. The resulting stabilized and aligned recording was transferred to Imaris for cell segmentation (middle panel) and extraction of corresponding fluorescence traces (right panel). Traces of neurons responding to sucrose 500mM in a representative recording. Steps performed in Imaris and in RStudio.

Supplementary Video 1: Whole organ recording and cell segmentation.

The TOG (larval main peripheral taste organ) recorded using genetically encoded GCaMP reporter in all neurons. The second fluorophore, nuclear RFP, is used for cell segmentation, allowing creation of spots corresponding to each individual neuron. GCaMP fluorescence intensity over time for each spot is represented by spot color, ranging from blue (low signal) to red (high intensity).

Figure 2: Taste neurons show high proportions of taste multimodality and opposed valence integration.

A. GSN responses to series of individual tastants. Illustrative cell responses (y axis) for each tastant series (x axis). Colors were scaled to reflect the intensity of activation to the given taste. Only responses above 20% DF/F were taken into account. Taste stimulation

885   was done with 5 tastants per animal, each belonging to one of the 5 canonical taste

886   modalities represented along the x axis: sweet (shades of red), bitter (blue), salt (purple),

887   amino acids (brown) and sour (yellow). We used 2 different series of taste recordings.

888   Series 1 consisted of sucrose 500mM for sweet taste, denatonium 10mM for bitter, NaCl

889   1M for high salt, valine 100mM as amino acid and citric acid 100mM for sour taste;

890   correspondingly, the second series consisted of sucrose 500mM, quinine 5mM, Nacl

891   100mM for low salt, arginine 100mM and citric acid 100mM. 7 separate organs were

892   recorded within the first series and 8 within the second (N=15). Total percentages of taste

893   integration per neuron per animal are represented on the pie chart: 66% of total

894   responding neurons were activated by only one tastant per organ and up to 34% of

895   neurons responded to more than one tastant. Most unimodal responses (uni-taste / cell,

896   left bar-chart) were recorded to sucrose and to high salt. Conversely, different

897   combinations of taste categories were observed to activate single neurons, with different

898   frequency of occurrence (multi-taste / cell, right bar-chart). The most frequent

899   combinations of taste modalities per cell per animal were sweet + amino acid, sweet +

900   sour, sour + high salt, sweet + high salt and sweet + bitter. Some of these combinations

901   involve a presumed positive valence (sucrose/sweet) taste together with a negative

902   valence taste (bitter or high salt) sensed by the same neuron.

903   B. Stimulation with groups of tastants comprising 2 sugar categories (mono and

904   disaccharides), low and high salt concentration, 4 amino acid and 2 bitter groups.

905   Responses of above 20% DF/F intensity threshold were considered.

906   Upper panels: Among all neurons responding to sugar group stimulation, we observed a

907   comparable ratio of cells activated by only one sugar category and 25.4% activated by

908   both mono and disaccharides. For salt-responding neurons, a higher proportion showed

909   unique activation to high salt than to low salt concentration, and 20% neurons responded

910   to both categories. Amino acids split in 4 groups gave a rounded 62% to 38% ratio of uni-

911   to multi-group response integration, calculated among all amino acid-responding neurons.

912   Taking into account total responding neurons from animals stimulated with all 8 groups

913   resulted in 60% to 40% uni- to multi-modality group response integration.

914   Lower panels: Within the total number of bitter-responsive neurons, 55% were uniquely

915   activated by stimulation with DSoTC group and respectively 30% by QLSC group.

916   Integration between sweet and bitter taste has been calculated on responding neurons

917   from animals stimulated with 2 groups of each modality: we observed similar proportions

918   of taste cells responding only to bitter groups (30,3%), cells responding only to sugar

919   (39,4%) and cells responding to groups from both modalities (30,3%).

920

921   **Figure 3: GSNs can respond to taste through activation or deactivation.**

922   A. Illustration of a segmented TOG with two highlighted neighboring neurons (white

923   dots) called CDL1, labeled in red and corresponding red fluorescence traces, and

924   CDL2 with corresponding blue traces. When stimulated with citric acid 100mM CDL1

925   generally responds with a canonical activation of fluorescence intensity increase, while

926   the adjacent CDL2 responds with a simultaneous deactivation, or a fluorescence

927   intensity decrease.

928   B. Cutting connections between chemosensory organs and brain (left panel illustration)

929   did not abolish the synchronous activation-deactivation response to citric acid

930   stimulation observed in CDL1-CDL2 neuronal couple (right panel).

931

932   **Figure 4: Mapping neuronal responses shows a high level of taste multimodality.**

933   A. Manual matching of responding GSNs across recorded organs (N=15) stimulated with

934   series of individual tastants (Fig.2A). 21 neuronal identities displayed on the y-axis. The

935   total response frequency (freq) of each neuron is represented in shades of grey (darker for

936   higher frequency) and translates how often the given neuron has been recorded to respond

937   above 20% DF/F0. For each mapped neuron the activation (yellow-red colors) and

938   deactivation (light-dark blue colors) to a respective tastant is displayed as heatmap for

939   both frequency and amplitude of response. Frequency of response (ovals) shows how

940   consistently a mapped neuron responded to a particular tastant. Response amplitudes

941   (squares) were plotted only for frequencies above 20% (N≥3), scaled and reflected by

942   color intensity of squares. To ease overall interpretation, denatonium and quinine were

943   grouped under the label "bitter", and valine and arginine as "amino acid".

944   B. 3D representative visualization of matched neurons.

945   C. CDL1 is activated by sucrose, citric acid and high salt, responding most robustly (most

946   frequently) to citric acid (red square, upper panel). By contrast, CDL2 is activated by

947   sucrose and denatonium, eliciting fluorescence deactivation to sucrose, low salt and most

948   frequently to citric acid (red square, lower panel).

949   D. AC1 is potentially the previously characterized C6 based on the very particular anterior

950   position in the organ (as shown in Fig.1C) and on detected responses to sucrose and high

951   salt, as previously described (48).

952

953   **Figure 5: Single-cell RNA sequencing of chemosensory neurons.**

954   A. Single cell dissociation protocol; manual picking of the fluorescently labelled sense

955   organs. For chemosensory organ identification, green fluorescence can be driven in all

956   neurons by a pan-neuronal driver line or in a subpopulation as labeled by *Ir76b*. *RFP* as a

957   tag to *Orco*, olfactory co-receptor present in olfactory cells, labels only DOG.

958   B. Integrated data sets as a single object in Seurat, represented in an UMAP embedding. The

959   final dataset after processing contains 153 cells expressing neuronal markers such as

960   *Neuroglian (Nrg), Synaptobrevin (Syb)*, *neuronal Synaptobrevin (nSyb)* or *pebbled (peb)*.

961   C. *Odorant receptor co-receptor* (*Orco)* is expressed in the DOG and *proboscipedia (pb)* in

962   the TOG. Their molecular expression appears largely non-overlapping in single cells.

963   Immunostainings against the RFP-tagged *Orco* showed expression restricted to the DOG,

964   as expected; *pb* expression shown by anti-Pb staining at embryonic stage labels TOG but

965   not DOG neurons.

966

967   **Supplementary Figure 5: Single-cell RNA sequencing of chemosensory neurons.**

968   A. Schematic principle of DisCo (DeterminIStic CO-encapsulation) with optimized co-

969   encapsulation efficiency for minimal cell loss. DropSeq on a microfluidic chip

970   equipped with valves that allow single cells (arrow in a.) to be stalled in a designated

971   region (bottom square, b.) until a corresponding barcoded bead (arrow in b.) reaches a

972   second designated region (upper square, c.) for their concomitant release into an oil

973   droplet (d.).

974   B. Three data sets as biological and technical replicates were merged and filtered to

975   eliminate cells with high gene number (nGene) or high UMIs (nCount) as potential

976   indicator of doublets and cells with high mitochondrial gene expression as indicator of

977   apoptotic cells. Correlation between high gene number and high UMIs (nGene vs nCount)

978   was used for establishing filter thresholds. Integrated data was subset for neurons,

979   resulting in a dataset of 153 cells above 400 genes per cell.

980   C. UMAP embedding in Seurat was colored by cell cluster association of cells. Neuronal

981   marker *Syb* shows expression in both cell clusters*, while *Orco* and *pb* show distinct

982   expression roughly corresponding to the identified clusters.

983

Figure 6: Neurotransmitters of chemosensory neurons show broad or narrow expression.

A. *Choline acetyltransferase* (*ChAT*/*Cha*) labels all chemosensory neurons using a *Cha*-Gal4 driver (67) (left panels). Corresponding expression in UMAP embedding colored by expression (right panel). Scale bar, 10 µm.

B. *TH* or *pale* (*ple*) is a tyrosine hydroxylase on the dopamine synthesis pathway, expressed in 2 TOG neurons as shown by anti-TH antibody staining (left panels). Corresponding *ple* molecular expression (right panel). Scale bar, 10 µm.

C. *Vesicular glutamate transporter* (*VGlut*) shows restricted expression in 3 neurons, using a *VGlut*-Gal4 line (left panels). *VGlut* narrow expression reflected in the UMAP embedding (right panel). Scale bar, 10 µm.

D. Physiological responses of the 3 *VGlut* expressing cells stimulated with water as control and with eight tastants introduced earlier (Fig.2A & 4). Mann-Whitney statistical test was used for comparisons between responses to water and each tastant (Suppl.File3): TOG neuron (left panel) responded to sucrose and to valine; Mec (neuron localized anterior-laterally to TOG, middle panel) showed no responses distinct from water; DOG neuron (right panel) responded to sucrose. Data presented as mean + SEM (error bars) and dots represent individual responses from separate experiments.

1002

Supplementary Figure 6: *VGlut*-expressing TOG neuron does not co-localize with C2 or with C7.

VGlut-positive TOG neuron (**A.**) does not share identity with C2 (**B.**), C7 (**C.**) or C1 (**D.**), using corresponding Gal4 lines and comparing the number of GFP positive cells in separate versus crossed lines. Scale bars, 10 µm.

1008

1009   **Figure 7: Co-expression of neurotransmitter markers.**

1010   A. *DAT* and *Vmat* share expression in single cells (magenta dots, blue arrows), as

1011   transporters of dopamine and respectively monoamines, the later inclusive of the first.

1012   B. Double cholinergic and dopaminergic profile as illustrated by a few cells (blue arrows).

1013   C. Co-expression of GABAergic *GABA-B-R2* and serotonergic *5-HT2B* receptors.

1014   D. Neuropeptide *Nplp4* present in a few *VGlut*-positive cells.

1015   E. Neuropeptide *Nplp2* co-localizes with *Vmat* (blue arrows).

1016

1017   **Figure 8: Chemosensory neurons express mechanosensory markers.**

1018   A. *nan*-Gal4 labels 1 TOG and 1 DOG neuron (left panel), scarce expression mirrored by the

1019   UMAP embedding colored by expression (right panel). Scale bar, 10 μm.

1020   B. *nompC*-Gal4 has been identified in 3 chemosensory cells (left panel), paralleled by

1021   UMAP embedding (right panel). Scale bar, 10 μm.

1022   C. *pain*-Gal4 labels a larger subpopulation of TOG neurons. We recorded neuronal response

1023   of *pain*-expressing neurons pre-exposed to water: mechanical stimulation produced by

1024   water pump switch ON/OFF. Responding cells in a 3D representation and respective

1025   fluorescence traces. Representative traces for 3 cells, each from two different animals.

1026

1027   **Supplementary Figure 8: Response to both gustatory and mechanical stimulation in a**

1028   **TOG neuron.**

1029   CM1 cell identified in a pan-neuronal whole-organ recording responds to sucrose 500mM

1030   and is deactivated when the water flow pump is turned on. The cell was already exposed

1031   to water inside the microfluidic channel, and therefore the response is likely not

1032   determined by water itself but by shear stress on the cell membrane.

1033

1034   **Supplementary Table 1. Chemicals used for taste stimulation.**

1035   **Supplementary File 1. Data referring to Fig.2.**

1036   **Supplementary File 2. Data referring to Fig.4.**

1037   **Supplementary File 3. Data referring to Fig.6C.**

1038   **Supplementary File 4. Whole organ calcium imaging, data processing, Suppl.Fig1 –**
1039   **ImageJ scripts and pipeline instruction files.**

Figure 1: Individual neurons of the TOG
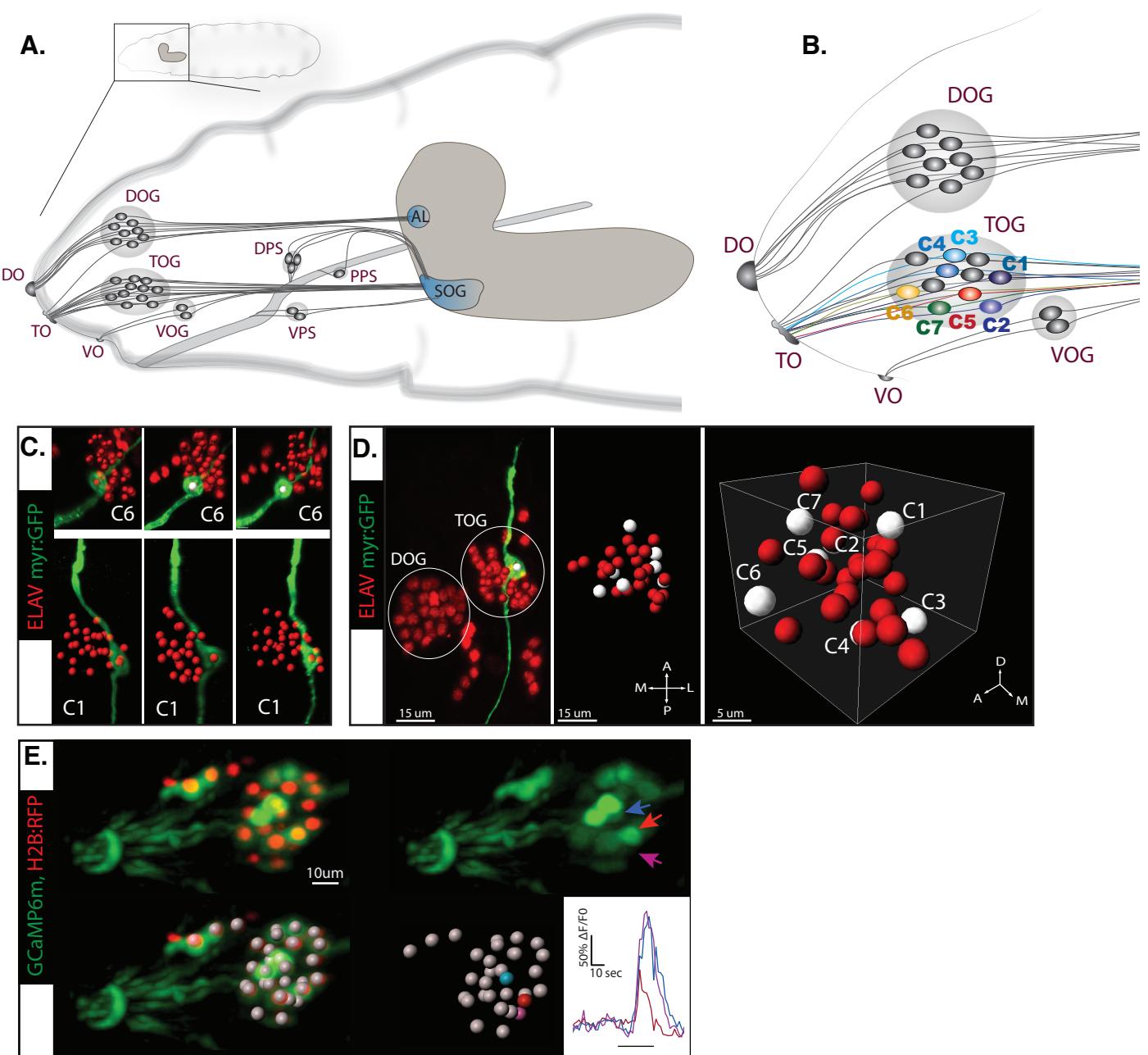
Supplementary Figure 1: Whole-organ recording -data processing.
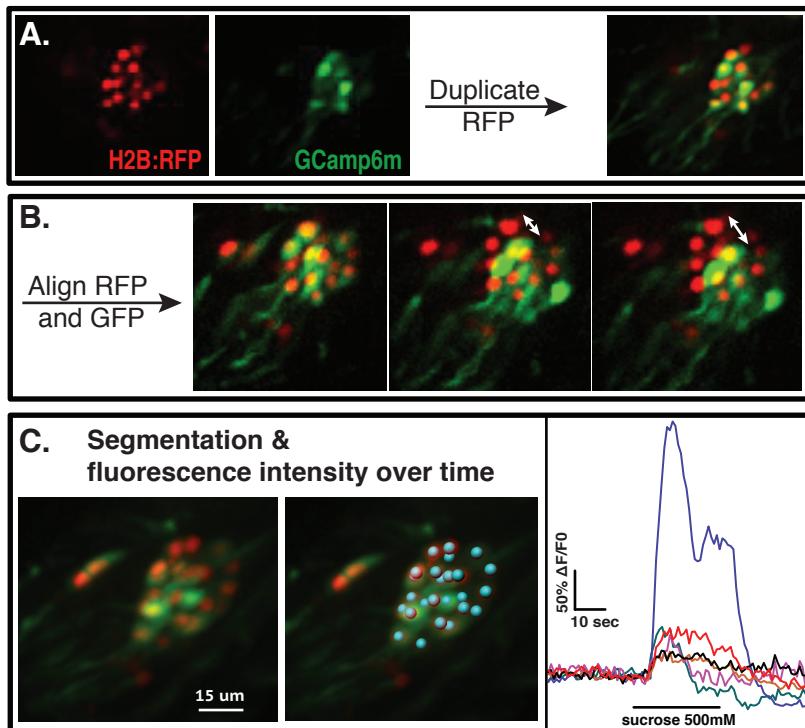
Figure 2: Tunning of response.

A. GSN responses to series of individual tastants.
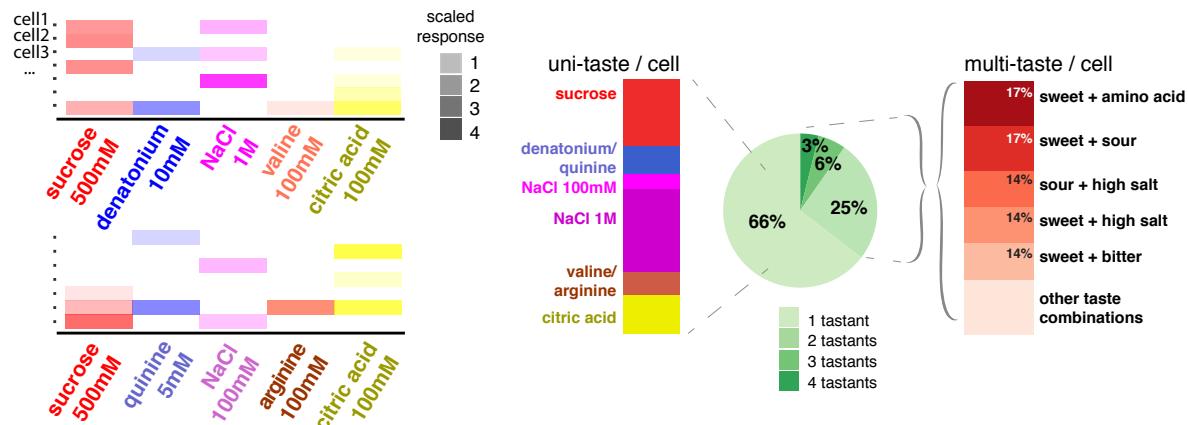
B. GSN responses to taste groups.
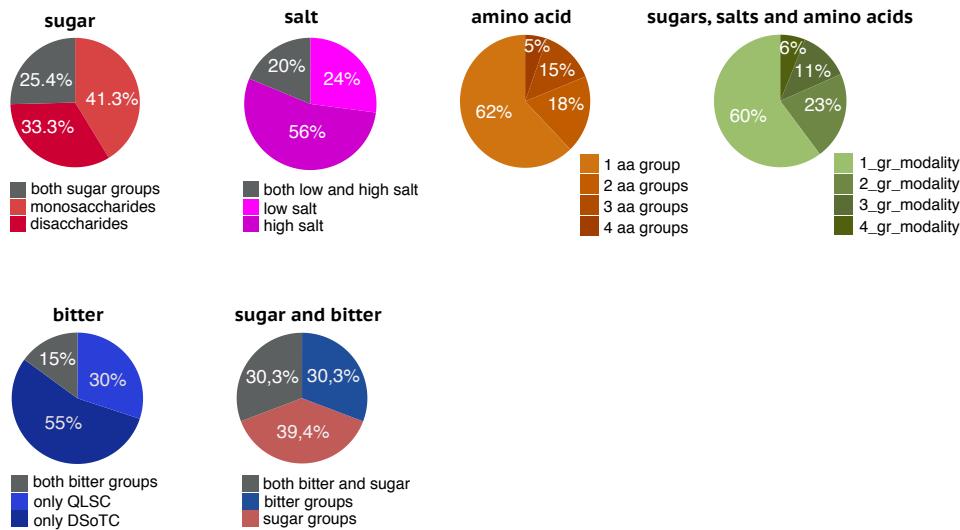
Figure 3: Activation and deactivation responses in taste neurons.
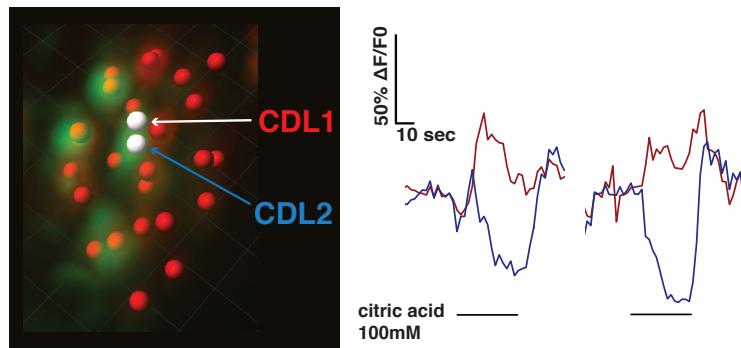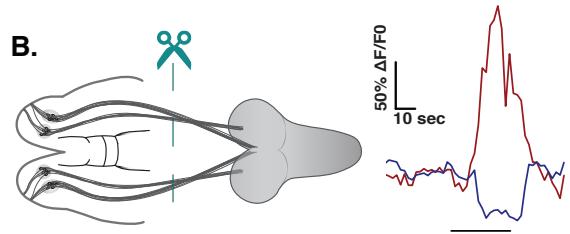
## Figure 4: Map of intensity and frequency of response.
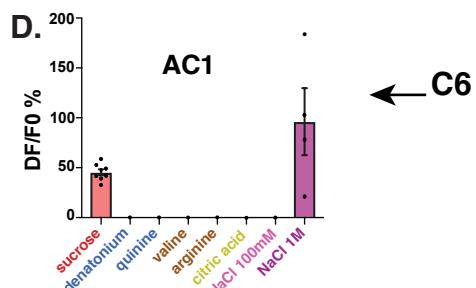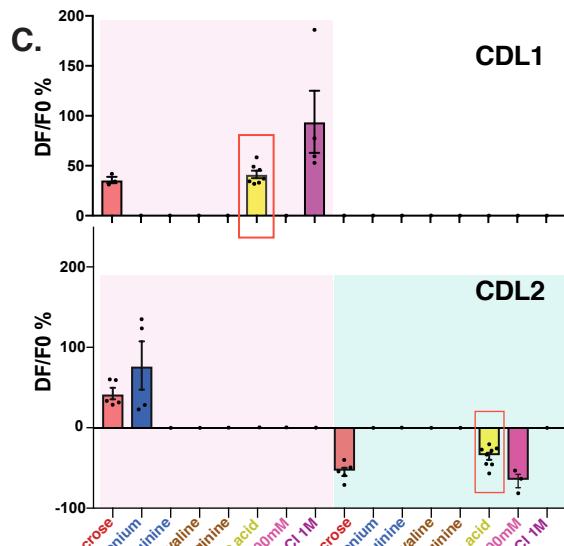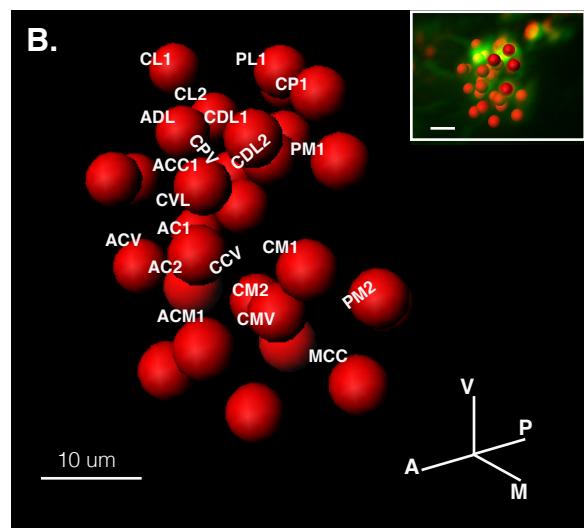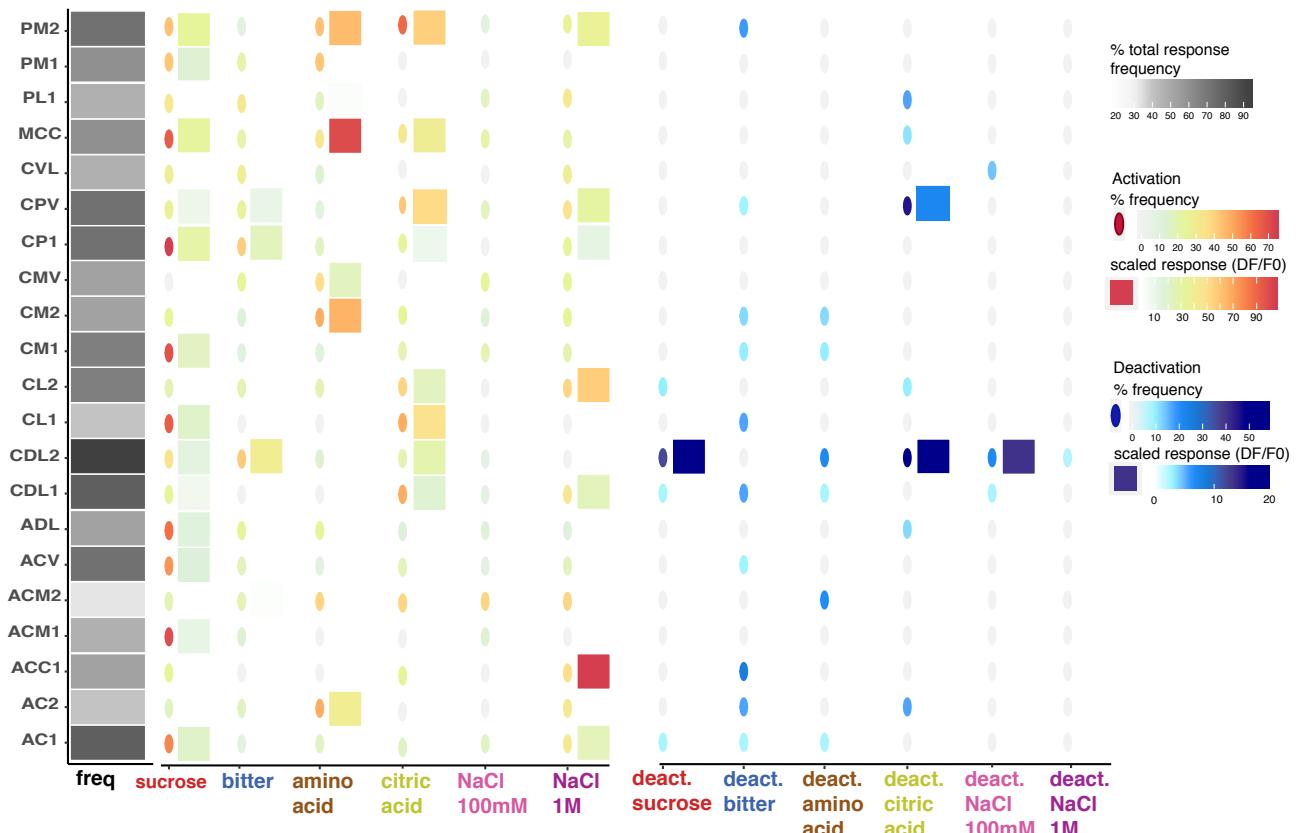
**Figure 5: Single cell RNA sequencing of chemosensory neurons.**
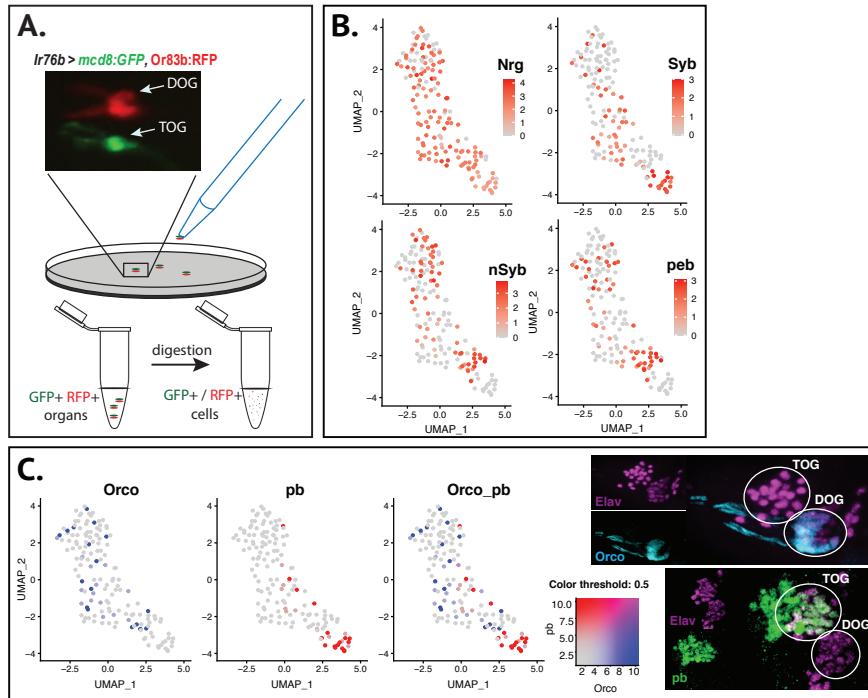
## Supplementary Figure 5: Single cell RNA sequencing of chemosensory neurons.
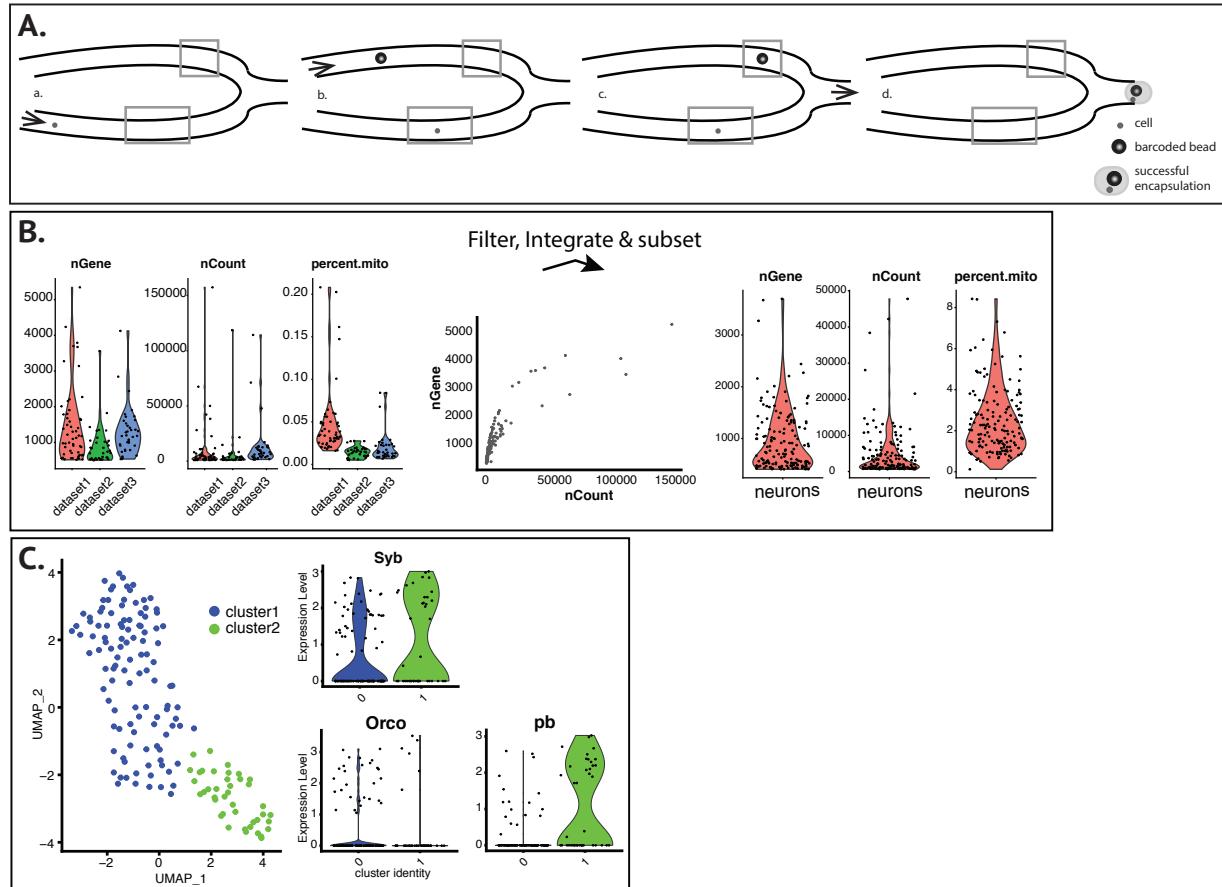
## Figure 6: Neurotransmitters of chemosensory neurons show broad or narrow expression
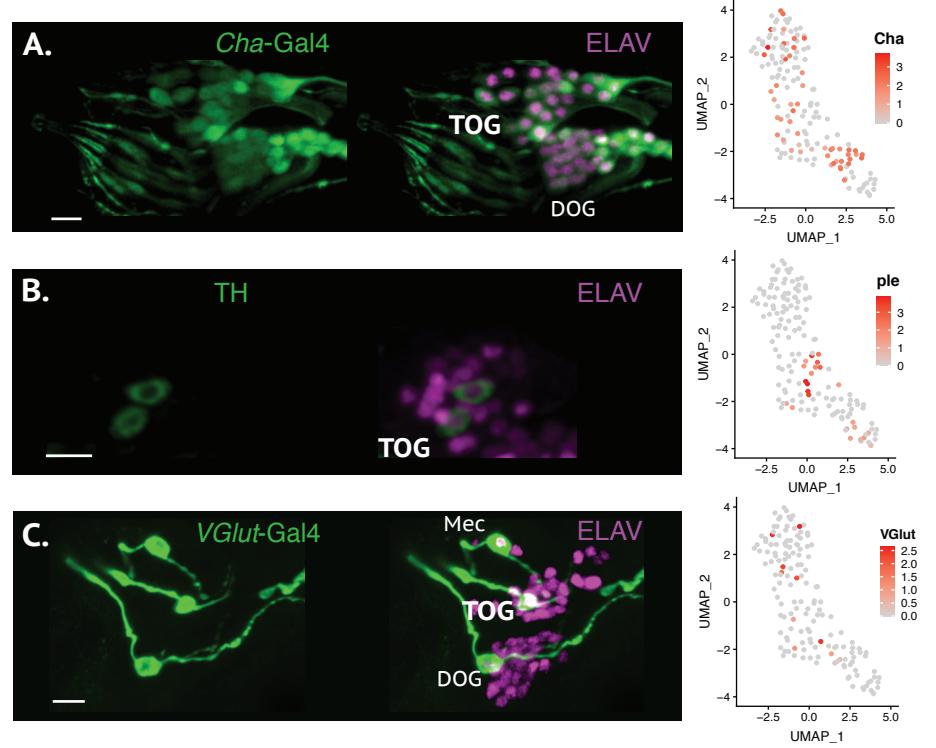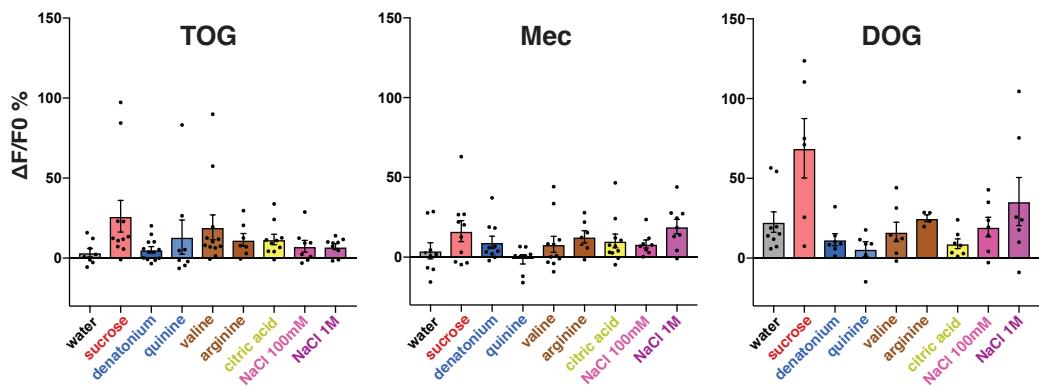
Supplementary Figure 6: *VGlut*-positive TOG neuron doesn't share identity with C2, C7 or C1 neurons.
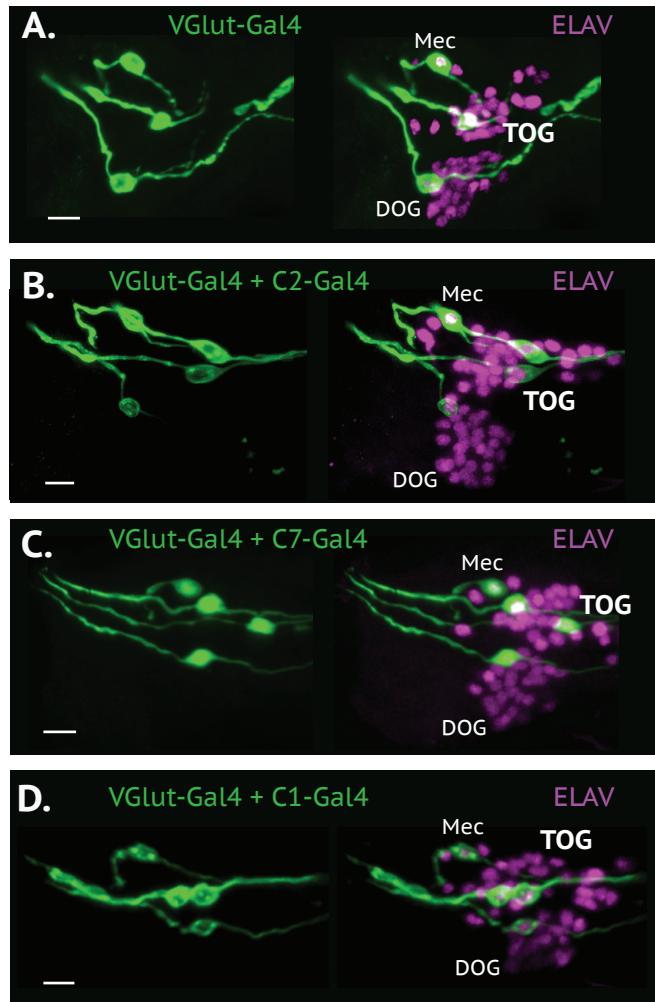
Figure 7: Co-expression of neurotransmitter marker genes.
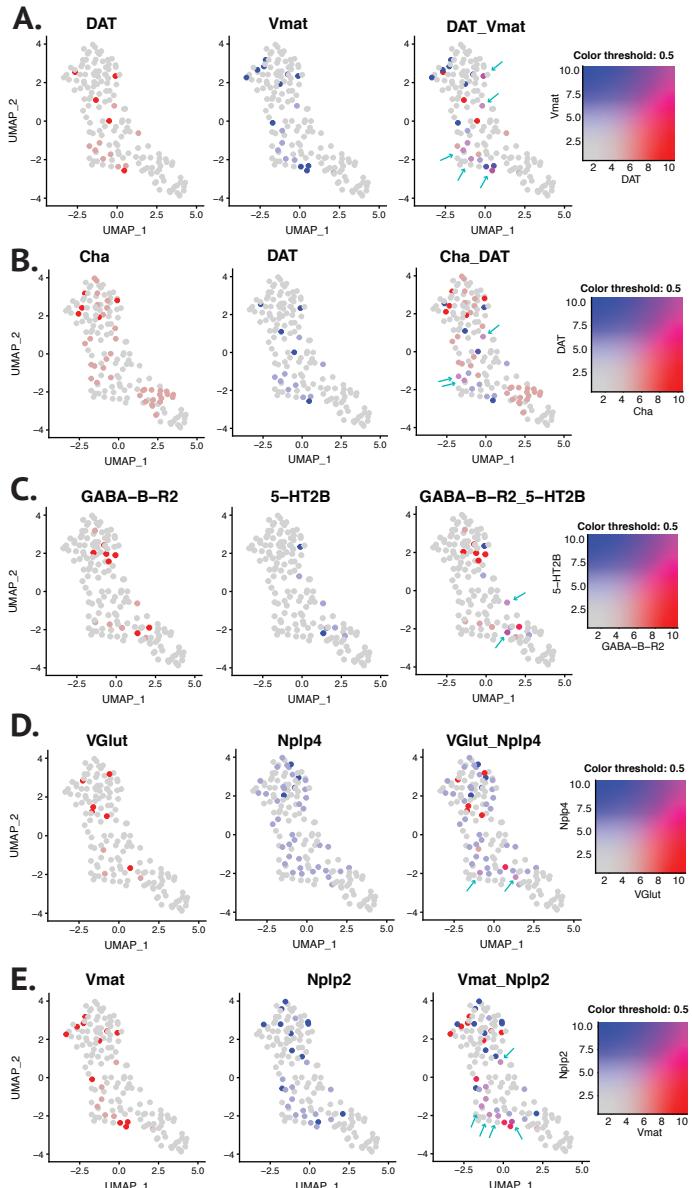
Figure 8: Chemosensory neurons express mechanosensory markers
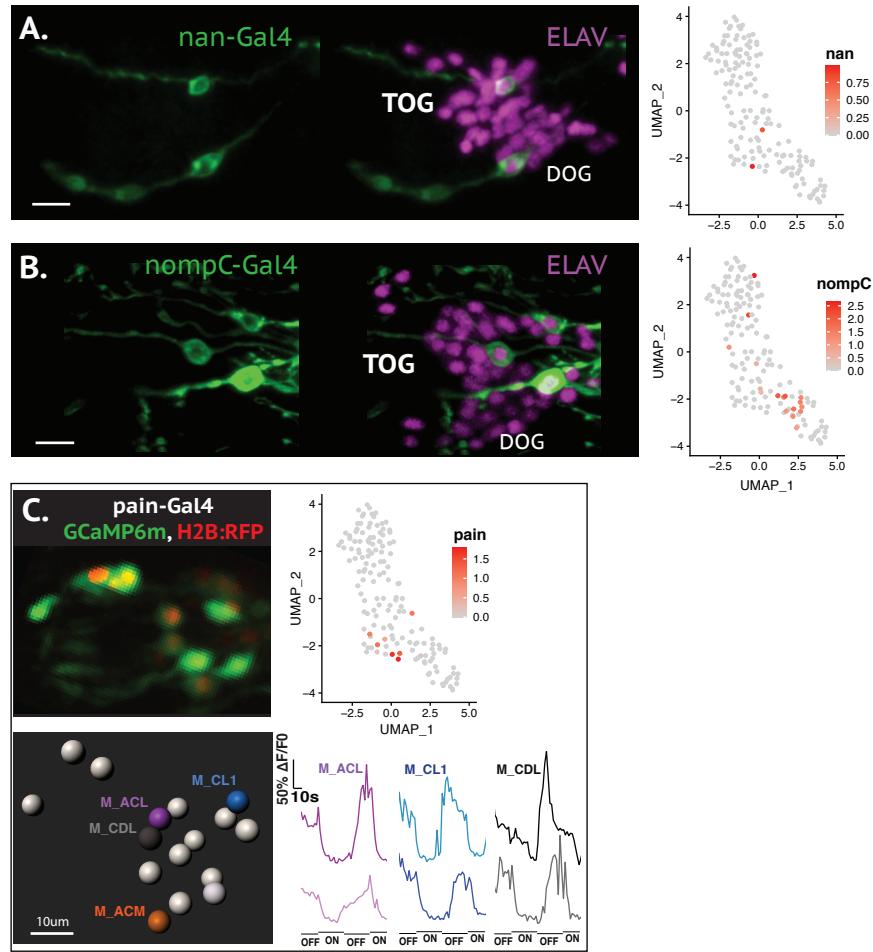
Supplementary Figure 8: Response to both gustatory and mechanical stimulation in a TOG neuron.